MCB
Journals.ASM.org

Plk1 Phosphorylation of PTEN Causes a Tumor-Promoting Metabolic State

Zhiguo Li,[a] Jie Li,[a] Pengpeng Bi,[b] Ying Lu,[a] Grant Burcham,[c] Bennett D. Elzey,[c] Timothy Ratliff,[c,e] Stephen F. Konieczny,[d,e] Nihal Ahmad,[f] Shihuan Kuang,[b,e] Xiaoqi Liu[a,e]

Department of Biochemistry, Purdue University, West Lafayette, Indiana, USA[a]; Department of Animal Sciences, Purdue University, West Lafayette, Indiana, USA[b]; Department of Comparative Pathobiology, Purdue University, West Lafayette, Indiana, USA[c]; Department of Biological Sciences, Purdue University, West Lafayette, Indiana, USA[d]; Purdue Center for Cancer Research, Purdue University, West Lafayette, Indiana, USA[e]; Department of Dermatology, University of Wisconsin, Madison, Wisconsin, USA[f]

One outcome of activation of the phosphatidylinositol 3-kinase (PI3K) pathway is increased aerobic glycolysis, but the upstream signaling events that regulate the PI3K pathway, and thus the Warburg effect, are elusive. Increasing evidence suggests that Plk1, a cell cycle regulator, is also involved in cellular events in addition to mitosis. To test whether Plk1 contributes to activation of the PI3K pathway, and thus aerobic glycolysis, we examined potential targets of Plk1 and identified PTEN as a Plk1 substrate. We hypothesize that Plk1 phosphorylation of PTEN leads to its inactivation, activation of the PI3K pathway, and the Warburg effect. Our data show that overexpression of Plk1 leads to activation of the PI3K pathway and enhanced aerobic glycolysis. In contrast, inhibition of Plk1 causes markedly reduced glucose metabolism in mice. Mechanistically, we show that Plk1 phosphorylation of PTEN and Nedd4-1, an E3 ubiquitin ligase of PTEN, results in PTEN inactivation. Finally, we show that Plk1 phosphorylation of PTEN promotes tumorigenesis in both its phosphatase-dependent and -independent pathways, revealing potentially new drug targets to arrest tumor cell growth.

Whereas normal cells generate ATP via mitochondrial respiration, tumor cells tend to metabolize glucose to lactate even in the presence of sufficient oxygen (the Warburg effect) (1). However, the molecular mechanisms underlying the Warburg effect are still elusive. The phosphatidylinositol 3-kinases (PI3Ks) are responsible for generation of the second messenger phosphatidylinositol 3,4,5-triphosphate (PIP3) from phosphatidylinositol 4,5-bisphosphate (2). In response to insulin/insulin-like growth factor 1 (IGF-1)-mediated activation of the insulin receptor/IGF-1 receptor (IR/IGF-1R), PI3K leads to elevation of PIP3, which activates AKT. Activated AKT mediates the subsequent phosphorylation and activation of the mTOR complex, which plays a critical role in the regulation of protein translation and metabolism (3). AKT is negatively regulated by the tumor suppressor PTEN (phosphatase and tensin homologue), which dephosphorylates PIP3 (4). Therefore, PTEN acts as a direct antagonist to the PI3K pathway. AKT activates mTOR via a double-negative mechanism. AKT phosphorylates and inhibits the function of TSC2, a GTPase-activating protein. TSC2 inactivates the small G protein Rheb, an activator of mTOR. Activated mTOR contributes to aerobic glycolysis via either increased protein expression of the glucose transporters GLUT1/3/4 (5) or pyruvate kinase M2 (PKM2) (6).

PTEN acts as a direct antagonist to the PI3K pathway, whose activation has well-established roles in the Warburg effect. PTEN is phosphorylated at the C terminus. Among the six known phosphorylation sites (T366, S370, S380, T382, T383, and S385), S385 is the primary site (7). Although casein kinase 2 (CK2) phosphorylates PTEN-S385 *in vitro*, no evidence has shown that CK2 is responsible for PTEN-S385 phosphorylation *in vivo* (7). Regulation of PTEN by phosphorylation is complex. First, phosphorylation of PTEN acts as an inhibitory switch by preventing its recruitment into a protein complex (8). Phosphorylated PTEN exists in a monomeric "closed" conformation and has low affinity for its interacting proteins. Conversely, unphosphorylated PTEN exists in an "open" conformation and has high binding affinity for its interacting proteins (8). Second, phosphorylation of the PTEN tail enhances its protein stability (9). Therefore, phosphorylated and stabilized PTEN is actually 3-fold less active in terms of its lipid phosphatase activity due to lack of interaction with its partners (8).

PTEN is localized predominantly to the nucleus in primary cells, but its nuclear localization is markedly reduced in cancer cells. Indeed, the absence of nuclear PTEN may serve as a prognostic indicator (10). Nuclear PTEN functions, such as regulation of the anaphase-promoting complex (APC) (11), are independent of its phosphatase activity. Nedd4-1, the major E3 ubiquitin (Ub) ligase of PTEN, regulates both PTEN nuclear import and stability. Although Nedd4-1-dependent monoubiquitination of PTEN allows its nuclear import, Nedd4-1-mediated polyubiquitination of PTEN leads to its degradation (12). Nedd4 family-interacting protein 1 (Ndfip1) is another factor that regulates PTEN nuclear import and ubiquitination. Ndfip1 binds to PTEN and promotes its nuclear import and ubiquitination in a Nedd4-1-dependent manner (13).

Polo-like kinase 1 (Plk1) is a regulator of many cell cycle-related events, including mitotic entry and bipolar spindle formation (14). A close correlation between Plk1 expression and carcinogenesis has been documented, and overexpression of Plk1 has

Received 16 June 2014 **Accepted** 17 July 2014
Published ahead of print 21 July 2014
Address correspondence to Xiaoqi Liu, liu8@purdue.edu.

doi:10.1128/MCB.00814-14
The authors have paid a fee to allow immediate free access to this article.

been found in many cancer cell lines and neoplastic tissues. Based on these findings, Plk1 has been proposed as a novel diagnostic marker for cancer, and its inhibition might represent a rewarding approach in cancer therapy (14). Indeed, several Plk1 inhibitors, including BI2536 and GSK461364, are in clinical studies for patients with various cancers (15). However, the molecular mechanisms responsible for these encouraging observations are still undefined. Here, we provide evidence that Plk1 phosphorylation of PTEN results in the Warburg effect and tumorigenesis.

MATERIALS AND METHODS

Cell culture and transfections. HPDE6 and RWPE1 cells were maintained in keratinocyte- and serum-free medium supplemented with human recombinant epithelial growth factor (5 ng/ml) and bovine pituitary extract (0.05 mg/ml). MCF10A cells were maintained in F-12–Dulbecco's modified Eagle's medium (DMEM) (50/50) supplemented with 5% horse serum, 20 ng/ml epidermal growth factor (EGF), 0.5 μg/ml hydrocortisone, 100 ng/ml cholera toxin, and 10 μg/ml insulin. HCEC-1CT cells were maintained in DMEM-Medium 199 (4:1) supplemented with 2% cosmic calf serum, 25 ng/ml EGF, 1 μg/ml hydrocortisone, 10 μg/ml insulin, 2 μg/ml transferrin, 5 nM sodium selenite, and 50 μg/ml gentamicin sulfate. DU145, Panc1, and HEK293T cells were cultured in DMEM supplemented with 10% fetal bovine serum (FBS), 100 units/ml penicillin, and 100 units/ml streptomycin at 37°C in 8% CO_2. PC3 cells were cultured in RPMI medium supplemented with 10% FBS. Plasmid transfections were performed with Lipofectamine (Invitrogen), whereas small interfering RNA (siRNA) was transfected with Transmessenger transfection reagent (Qiagen). Cells were examined 30 h after transfection for immunoblotting (IB).

Plasmids and RNA interference (RNAi). The lysine-free Ub (KØ-Ub) construct was kindly provided by Pier Paolo Pandolfi at Harvard Medical School. The PTEN expression plasmid was subcloned into pEGFP-C1, and its derivatives were created with the QuikChange site-directed mutagenesis kit (Stratagene). The identities of all plasmids were confirmed by sequencing. The pKD-CK2 construct used to deplete CK2 was obtained from Upstate. The following target sequence was used to design siRNA against human Plk1: AAGGGCGGCTTTGCCAAGTGCTT.

Antibodies and reagents. The phosphospecific antibody against Nedd4-1-S328 was generated by Proteintech. In brief, a peptide containing phosphorylated S328 (pS328) was synthesized and used to immunize rabbits. After the antibodies were affinity purified, a series of control experiments were performed to confirm its specificity. The antibodies against PTEN (9188), pS380-PTEN (9551), pS380/T382/T383-PTEN (9554), pAKT (4060), AKT (9272), PKM2 (3198), and pS6 (2211) used in this study were purchased from Cell Signaling. The antibodies against Plk1 (sc-17783) and CK2α were from Santa Cruz Biotechnology, whereas the antibodies against pS385-PTEN (NG1828769) and poly(ADP-ribose) polymerase (PARP) (NG1923455) were from Millipore. The antibodies against pS370-PTEN (ab30654), glutaminase (GLS) (ab60709), and 6-phosphofructo-2-kinase/fructose-2,6-biphosphatase isoform 3 (PFKFB3) (ab96699) were purchased from Abcam. MG132 (carbobenzoxy-L-leucyl-L-leucine) was obtained from EMD Bioscience and used at 10 μM. To inhibit Plk1 and PTEN in mice, the following conditions were used: BI2536 at 10 mg/kg body weight and VO-OH at 0.2 mg/kg body weight. To inhibit mTOR in cultured cells, 20 nM rapamycin was used.

Immunoblotting and immunoprecipitation (IP). Cell lysates were prepared in TBSN buffer (20 mM Tris-HCl, pH 8.0, 1 mM EDTA, 0.5 mM Na_3VO_4, 5 mM EGTA, 1% NP-40) supplemented with 150 mM NaCl. For IP, lysates were incubated with antibodies in TBSN at 4°C overnight, followed by 3 washes with TBSN plus 500 mM NaCl and 3 more washes with TBSN plus 150 mM NaCl.

Adenovirus preparation. Adenovirus was generated using the pAdEasy XL adenoviral vector system (Stratagene, La Jolla, CA) based on the manufacturer's instructions. To determine the titers of the virus stocks, serial dilutions were made, and individual 1-ml dilutions were incubated with 293A cells at 37°C for 2 days to infect the cells. Two days after infection, the green fluorescent protein (GFP)-positive cells were counted and the viral titers were calculated.

Recombinant protein purification. Various glutathione *S*-transferase (GST)-tagged PTEN or Nedd4-1 constructs were subcloned into pGEX-KG and expressed in *Escherichia coli* strain BL21(DE3). The GST fusion proteins were expressed by induction for 4 h at 37°C with 0.1 mM IPTG (isopropyl-β-D-thiogalactopyranoside) and purified using glutathione-Sepharose 4B beads according to the manufacturer's instructions.

Plk1 kinase assay. Purified recombinant PTEN or Nedd4-1 was incubated with purified wild-type (WT) Plk1 or Plk1-K82M in kinase reaction buffer [50 mM Tris, pH 7.5, 10 mM $MgCl_2$, 2 mM EGTA, 0.5 mM Na_3VO_4, 100 mM 4-nitrophenyl phosphate di(tris) salt (PNPP), 25 mM dithiothreitol (DTT), 125 μM ATP] supplemented with 10 μCi of [γ-^{32}P]ATP at 30°C for 30 min. After the reaction mixtures were resolved by SDS-PAGE, the gels were stained with Coomassie brilliant blue, dried, and subjected to autoradiography.

Measurement of glucose, lactate, and glutamine. Cells were seeded in culture plates and cultured for 48 h after virus infection or transfection. The culture media were collected to measure the levels of glucose, lactate, and glutamine with a glucose assay kit (Eton Bioscience), a lactate assay kit (Eton Bioscience), and a glutamine/glutamate determination kit (Sigma), respectively, and normalized to the cell number.

***In vivo* ubiquitination assay.** 293T cells were cotransfected with plasmids expressing hemagglutinin (HA)-ubiquitin, GFP-PTEN, and Flag-Plk1 (T210D or K82M). Forty-eight hours after transfection, the cells were treated with MG132 and harvested for IP with the antibodies indicated in each experiment, followed by IB.

Glucose and insulin tolerance tests. All procedures involving mice were performed with the approval of the Purdue University Animal Care and Use Committee. The mice were housed in the animal facility with free access to standard rodent chow and water. Glucose and insulin tolerance tests (GTT and ITT) were performed after intraperitoneal (i.p.) injection of glucose or insulin, respectively. GTT were performed by injection of D-glucose (Sigma) at a dose of 2 mg/g body weight after an overnight fast. For ITT, insulin (0.5 U/kg of body weight) was injected into fasting mice. Blood glucose levels were then measured at different times (15 min, 30 min, 45 min, 60 min, 75 min, and 90 min) after injection with a Onetouch Ultra glucometer (Lifescan, Mountain View, CA).

Measurement of energy expenditure. Oxygen consumption (VO_2), carbon dioxide production (VCO_2), and the respiratory exchange ratio (RER) (VCO_2/VO_2) were measured under a consistent environmental temperature and light cycle using an indirect calorimetry system (Oxymax; Columbus Instruments). After the mice were acclimated to the metabolic chamber for 2 days, VO_2 and VCO_2 were measured in individual mice at 15-min intervals during a 48-h period.

Soft-agar assay. Cells were seeded on soft agar in 6-well plates at a density of 1×10^3 cells per well and cultured for 3 weeks at 37°C under 5% CO_2. The dishes were stained with 0.005% crystal violet, and colonies were scored.

Mouse xenograft model. PC3 cells (5×10^6 cells per mouse) expressing different forms of GFP-PTEN were mixed with an equal volume of Matrigel (Collaborative Biomedical Products) and inoculated into the flanks of athymic nude mice (Harlan Laboratories). The sizes of the tumors were followed for 3 weeks before the animals were sacrificed. Tumor volumes (estimated using the following formula: $V = L \times W^2/2$, where V is volume, L is length, and W is width) were measured every other day with a digital caliper.

Measurement of metabolic intermediates with LC-MS. To prepare extracts, cells (2×10^6 to 6×10^6) were quickly quenched with 25 ml cold 60% methanol. After incubation in the cryostat bath (−45°C) for 3 min, the mixtures were centrifuged at 2,000 × *g* for 5 min at −20°C, and the cell pellets were resuspended in 5 ml of cold quenching solution (−45°C), followed by a second identical centrifugation. To extract the metabolites, tubes containing cell pellets were placed into a 90°C water bath and im-

mediately overlaid by a solution of 75% (vol/vol) boiling ethanol. After 3 min incubation, the tubes were transferred to a −80°C freezer until further analysis. The high-performance liquid chromatography (HPLC)–electrospray ionization (ESI)–mass spectrometry (MS) system (Agilent), consisting of a capillary 1100 series HPLC system and an ESI source and time of flight (TOF) mass spectrometer, is controlled by ChemStation software. Separations were performed on a Zorbax C_8 column (2.1 mm by 150 mm) with the autosampler setting at 10°C. The elution started from 95% mobile phase A (5 mM tetrabutylammonium [TBA] aqueous solution adjusted to pH 5.0 with acetic acid) and 5% mobile phase B (100% acetonitrile [ACN]) and was raised to 70% B in 25 min and further raised to 100% B in 2 min and then held at 100% B for 3 min. The flow rate was set at 0.3 ml/min, with an injection volume of 20 μl. Liquid chromatography (LC)-ESI-MS chromatograms were acquired in negative ion mode under the following conditions: capillary voltage, 4,000 V; fragmenter, 165 V; dry temperature, 300°C; dry-gas flow maintained at 8 liters/min; and acquisition range, *m/z* 150 to 1,000. To monitor metabolites, individual standard metabolite solutions (each 0.1 mM) were separately labeled with aniline and [$^{13}C_6$]aniline, and a 1:1 mixture was analyzed. The LC peak and MS spectrum patterns were examined to confirm the labeling reaction and to obtain the *m/z* value for sample analysis. A 14.3 μM standard mixture including 33 analytes was used for optimizing the labeling and separation conditions. To determine the detection limit and linearity range, a mixture of 33 analytes at various concentrations for each component (depending on its MS response intensity) was prepared. A series of dilutions from this mixture were labeled with aniline. Another aliquot of the mixture was labeled with aniline-13C6, and a certain amount of this derivative mixture was added to the above-mentioned series of solutions as references for MS response calibration.

Statistical analysis. All data are presented as means and standard deviations (SD). Statistical calculations were performed with Microsoft Excel analysis tools. A two-tailed, unpaired Student *t* test was used to assess the difference between the effects of treatment in cell lines. One-way analysis of variance was used to determine statistically significant differences from the mean in the animal study. *P* values of <0.05 were considered statistically significant.

RESULTS

Plk1 regulates the PI3K pathway. Because the phosphorylation status of several members of the PI3K pathway is regulated by Plk1-associated activity (16–18), we decided to test whether Plk1 regulates this pathway. Accordingly, we first showed that BI2536, a Plk1 inhibitor (19), reduced the phosphorylation level of S6 in mimosine-treated DU145 prostate cancer cells (Fig. 1A). Addition of mimosine, a drug that causes cell cycle arrest at G_1, ensured that cells were at the same stage of the cell cycle. Next, we showed that depletion of Plk1 also inhibited activation of the PI3K pathway in Panc1 pancreatic cancer cells, revealing a universal role for Plk1 in different cancer lines (Fig. 1B). Furthermore, depletion of Plk1 also antagonized insulin- and IGF-1-induced activation of the PI3K pathway in Panc1 cells (Fig. 1C and D). We are aware that depletion of Plk1 leads to G_2/M arrest in cancer cells (20). Thus, to rule out a cell cycle effect, we used an adenovirus-based approach to overexpress GFP-Plk1 in four nontransformed cell lines, as modification of Plk1 in normal cells does not induce cell cycle defects (20, 21). The cell lines used were HPDE6, a human pancreatic duct epithelial cell line with a nearly normal genotype and phenotype (22); HCEC-1CT, an immortalized human colonic epithelial cell line expressing Cdk4 and telomerase (23); MCF10A, an immortal cell line that arose spontaneously from mortal human diploid breast epithelial cells without virus or chemical intervention (24); and RWPE1, an immortal cell line originating from normal human prostate epithelium that does not form solid tumors when implanted into nude mice (25). Overexpression of Plk1 in all four cell lines led to activation of the PI3K pathway, as indicated by elevation of pAKT and pS6 levels (Fig. 1E to H). Further, we showed that $Plk1^{+/-}$ mouse embryonic fibroblasts (MEFs) had reduced phosphorylation levels of AKT and S6 in comparison to wild-type (WT) MEFs (Fig. 1I) and that reexpression of WT Plk1 but not the kinase-defective Plk1-K82M mutant rescues activation of the PI3K pathway (Fig. 1J). Thus, we conclude that Plk1 regulates the PI3K pathway.

Considering that Plk1 is a target of the E3 ubiquitin ligase APC/cyclosome-Cdh1 (APC/C-Cdh1), we also asked whether depletion of Cdh1 by lentivirus-based RNAi (26) phenocopies the Plk1 overexpression phenotype. As indicated, Cdh1 depletion led to stabilization of Plk1 and elevation of phosphorylation levels of AKT and S6 (Fig. 1K and L). Because PTEN is the major regulator of the PI3K pathway, we asked if Plk1-induced activation of the PI3K pathway was PTEN dependent. As shown in Fig. 1M, overexpression of GFP-Plk1 in PTEN-null PC3 cells did not lead to activation of the PI3K pathway. Similarly, overexpression of GFP-Plk1 did not affect the status of AKT phosphorylation in RWPE1 cells after PTEN depletion (Fig. 1N and O). Therefore, Plk1-induced activation of the PI3K pathway is PTEN dependent.

Plk1 regulates energy metabolism. Considering the critical role of the PI3K pathway in glucose metabolism, we next asked whether Plk1 overexpression affects this process. As indicated, overexpression of Plk1 led to increased glucose consumption and lactate production in HPDE6, HCEC-1CT, and MCF10A cells (Fig. 2A to C). In agreement with this, overexpression of Plk1 increased the level of PKM2, a critical regulator of aerobic glycolysis, in these cells (Fig. 1E to G). Furthermore, LC-MS analysis of metabolic intermediates indicated that depletion of Plk1 reduces the levels of glucose-6-phosphate (G-6-P), 3-phosphoglycerate (3-PG), and phosphoenolpyruvate (PEP), three intermediates of glycolysis (Fig. 2D), and the levels of fumarate, malate and α-ketoglutarate, three intermediates of the tricarboxylic acid (TCA) cycle (Fig. 2E). In contrast, a Plk1-induced Warburg effect was not observed in PTEN-null PC3 cells (Fig. 2F) or in PTEN-depleted RWPE1 cells (Fig. 2G).

To further test whether Plk1 is indeed involved in energy metabolism, we performed a series of experiments with mice. We first expressed GFP-Plk1 via intravenous injection of adenovirus, a protocol that has been used in viral-gene delivery (27). Reverse transcription (RT)-PCR results indicated that the liver is the major organ with a high level of Plk1 expression upon virus injection (data not shown). As indicated, expression of GFP-Plk1 resulted in activation of the PI3K pathway and elevation of PKM2 in the liver (Fig. 3A). Significantly, expression of Plk1 increased glucose uptake in a GTT (Fig. 3B). In an alternative approach, we transiently expressed Flag-Plk1 in the livers of adult mice using hydrodynamic tail vein injections, as described previously (28), and found that expression of Flag-WT Plk1 but not the kinase-dead K82M mutant led to an increase in the phosphorylation levels of AKT and PTEN-S385 (Fig. 3C). Moreover, expression of Flag-Plk1 enhanced glucose uptake in both GTT (Fig. 3D) and ITT (Fig. 3E) experiments. Third, we asked whether inhibition of Plk1 affects energy metabolism (Fig. 3F to H). In these experiments, mice were treated with BI2536 for 1 week, and no obvious phenotypes, including significant weight loss and reduced appetite, were observed after the treatment. As indicated, refeeding of starved mice activated the PI3K pathway, and pretreatment with BI2536

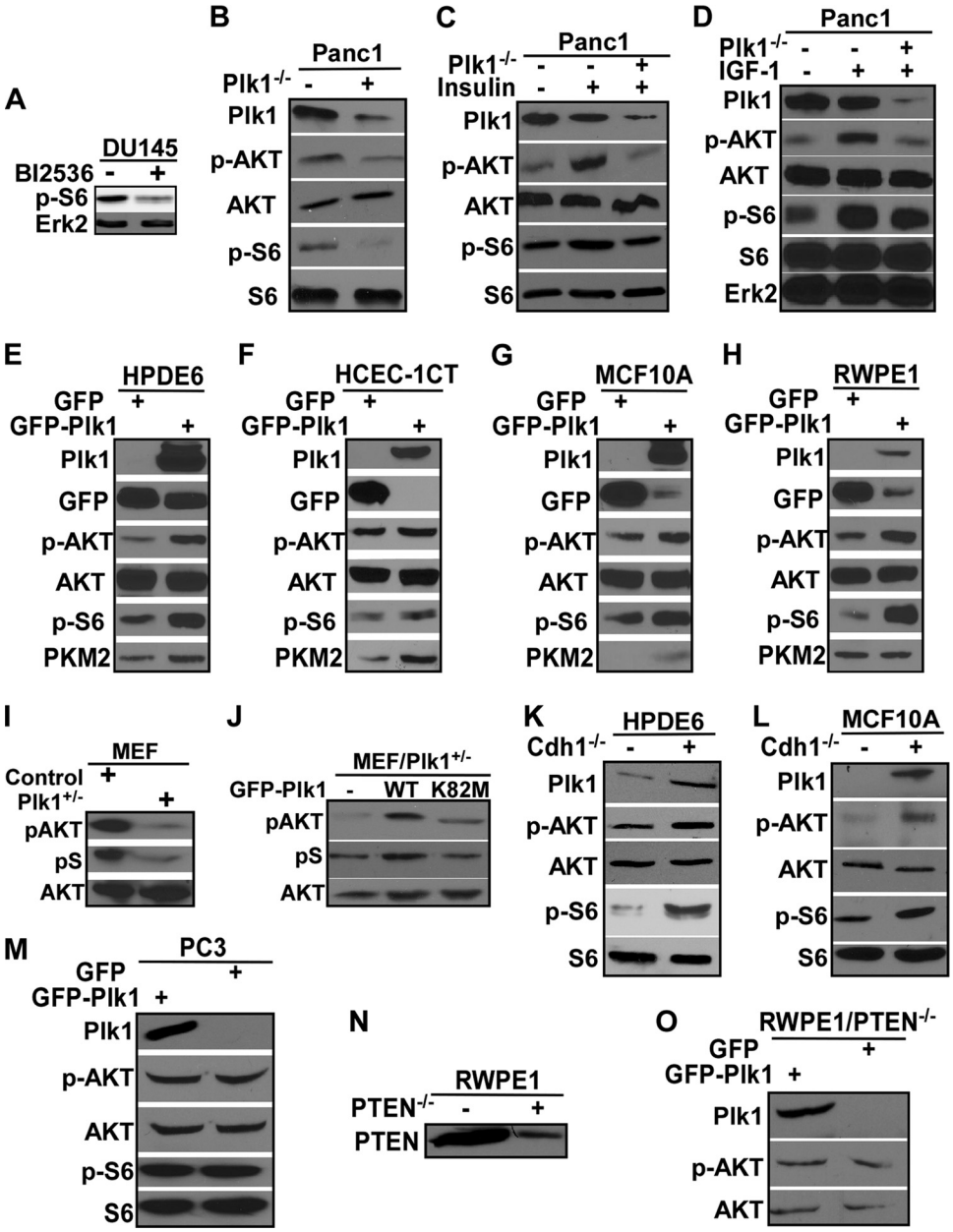

FIG 1 Plk1 acts upstream of the PI3K pathway. (A) Inhibition of Plk1 reduces the phosphorylation level of S6. DU145 prostate cancer cells were treated with 50 nM BI2536 for 8 h and harvested for anti-pS6 IB. The cells were also treated with mimosine to ensure they were all in the same stage of the cell cycle. (B to D) Depletion of Plk1 antagonizes activation of the PI3K pathway in Panc1 pancreatic cancer cells. Panc1 cells were depleted of Plk1 by RNAi and harvested (B) or serum starved for 24 h, treated with insulin (C) or IGF-1 (D) for 15 min, and harvested. (E to H) Overexpression of Plk1 activates the PI3K pathway in four nontransformed cell lines. HPDE6 (E), HCEC-1CT (F), MCF10A (G), and RWPE1 (H) cells were infected with adenovirus expressing GFP-Plk1 for 48 h. (I) Knockout of Plk1 inhibits the activity of the PI3K pathway in MEFs. MEFs (WT or $Plk1^{+/-}$) were subjected to IB. (J) Expression of GFP-WT Plk1 but not the kinase-defective Plk1-K82M mutant rescues the activity of the PI3K pathway in $Plk1^{+/-}$ MEFs. $Plk1^{+/-}$ MEFs were transfected with GFP-Plk1 (WT or K82M). (K and L) Cdh1 depletion leads to activation of the PI3K pathway. HPDE6 (K) and MCF10A (L) cells were infected with lentivirus to deplete Cdh1 and harvested for IB. (M) Overexpression of GFP-Plk1 does not affect the PI3K pathway in PC3 prostate cancer cells. PC3 cells were transfected with GFP-Plk1 and harvested for IB. (N and O) Overexpression of GFP-Plk1 in PTEN-depleted RWPE1 cells does not affect the PI3K pathway. RWPE1 cells were infected with lentivirus to deplete PTEN (N) and reinfected with adenovirus expressing GFP-Plk1 for 48 h (O).

antagonized this effect (Fig. 3F), confirming that Plk1 regulates the PI3K pathway. In agreement with the results based on the approaches that overexpress Plk1 (Fig. 3A to E), BI2536 treatment inhibited glucose uptake (Fig. 3G). Furthermore, indirect calorimetry analysis revealed that BI2536-treated mice showed lower energy expenditure than control mice, as indicated by both reduced CO_2 production and reduced O_2 consumption (Fig. 3H). In contrast, overexpression of Flag-Plk1 resulted in higher energy expenditure than control mice (Fig. 3I).

Finally, we tested whether Plk1-mediated regulation of glucose metabolism depends on the PI3K pathway. We first tested the role of PTEN, as Flag-Plk1 expression in mouse liver increased the

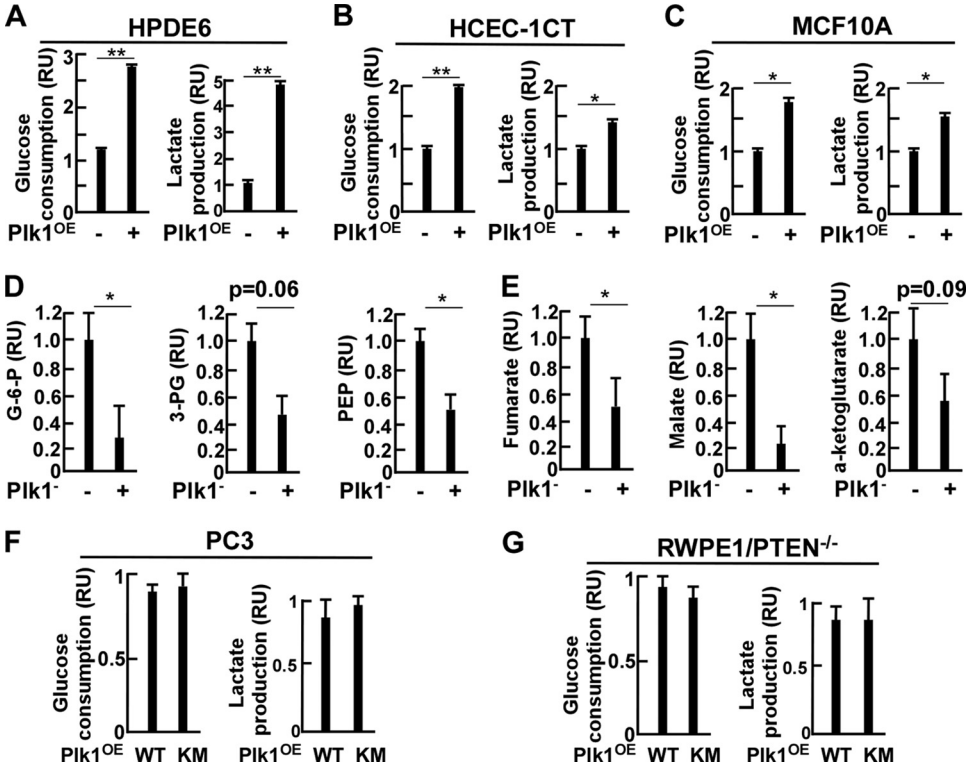

FIG 2 Plk1 overexpression results in the Warburg effect. (A to C) Overexpression of Plk1 promotes aerobic glycolysis. After HPDE6 (A), HCEC-1CT (B), and MCF10A (C) cells were infected with adenovirus to express Plk1 for 48 h, the media were collected for measurement of glucose consumption (left) and lactate production (right). RU, random units. (D and E) Plk1 knockdown alters glucose metabolism in 293T cells. Shown is quantification of metabolic intermediates in glycolysis (D) and the TCA cycle (E) at 70 h after depletion of Plk1. (F) Overexpression of Plk1 in PC3 cells does not affect glucose metabolism in PC3 cells. PC3 cells were transfected with GFP-Plk1 (WT or K82M) and harvested. (G) Overexpression of Plk1 does not affect glucose metabolism in PTEN-depleted RWPE1 cells. RWPE1 cells were depleted of PTEN and reinfected with adenovirus expressing GFP-Plk1. The data are presented as means and SD. *, $P < 0.05$; **, $P < 0.01$.

phosphorylation level of PTEN-S385 (Fig. 3C). As indicated, VO-OH, a PTEN inhibitor (29), antagonized the inhibitory effect of BI2536 on glucose uptake (Fig. 4A), suggesting that Plk1 regulates glucose metabolism via its activity toward PTEN. Second, a similar result was obtained with PTEN knockout mice (Fig. 4B). Third, we used liver-specific mTOR knockout mice (Fig. 4C and D) and showed that these mice lose their response to BI2536 in GTT experiments (Fig. 4E). Fourth, Plk1-induced glucose uptake can be reversed by rapamycin, an mTOR inhibitor, confirming a critical role of the PI3K pathway in increased glucose consumption due to Plk1 elevation (Fig. 4F).

Plk1 phosphorylates PTEN at S385. To understand how Plk1 regulates the PI3K pathway, we focused on PTEN. We first showed by coimmunoprecipitation experiments that overexpressed Plk1 binds to overexpressed PTEN (Fig. 5A and B). We then showed that Plk1 directly phosphorylates PTEN (Fig. 5C) at S385 (Fig. 5D and E). Plk1 phosphorylation of PTEN at S385 was confirmed by anti-pS385-PTEN IB (Fig. 5F). Moreover, the level of pS385 (phospho-PTEN-S385) was inhibited by BI2536, indicating that phosphorylation of PTEN-S385 is dependent on Plk1 activity in cells (Fig. 5G). Further, anti-pS385 detected phosphorylated PTEN in mitotic cell lysates but not from Plk1-inhibited cells, suggesting that endogenous PTEN is phosphorylated at S385 by Plk1 (Fig. 5H and I). Considering that CK2 is a PTEN kinase *in vitro* (7), we then depleted either Plk1 or CK2 with RNAi in cells expressing GFP-PTEN. Depletion of Plk1 significantly reduced the signal of pS385, confirming that Plk1 is indeed a kinase responsible for phosphorylation of PTEN-S385. In contrast, CK2 depletion did not affect the level of pS385 but slightly reduced the signal of pS370 (phospho-PTEN-S370), suggesting that CK2 might phosphorylate PTEN-S370 but not S385 (Fig. 5J). Finally, PTEN-S385 is conserved among different species, and the sequence context fits the consensus Plk1 phosphorylation site (Fig. 5K).

Plk1 phosphorylation of PTEN inhibits its polyubiquitination, degradation, and activity. Having established that Plk1 is responsible for PTEN-S385 phosphorylation, we next explored the functional significance of this phosphorylation event. Overexpression or inhibition of Plk1 resulted in an increased or decreased level of PTEN protein, respectively (Fig. 6A), suggesting that Plk1 might regulate the degradation of PTEN. In agreement with this, introduction of alanine mutants at S370, S380, or S385 resulted in a reduced level of PTEN (Fig. 6B). Further, we ectopically expressed various PTEN constructs at different known phosphorylation sites and measured the half-lives of these proteins. Introduction of aspartic acid or alanine mutations at S370, S380, T382, T383, or S385 resulted in stabilization or degradation of PTEN, respectively (Fig. 6C to G), indicating that phosphorylation of PTEN at different sites of the C terminus inhibits its degradation. Next, we asked whether Plk1-associated activity toward PTEN inhibits its polyubiquitination, a prerequisite of protein degradation, by cotransfection of Plk1 with different activities (T210D,

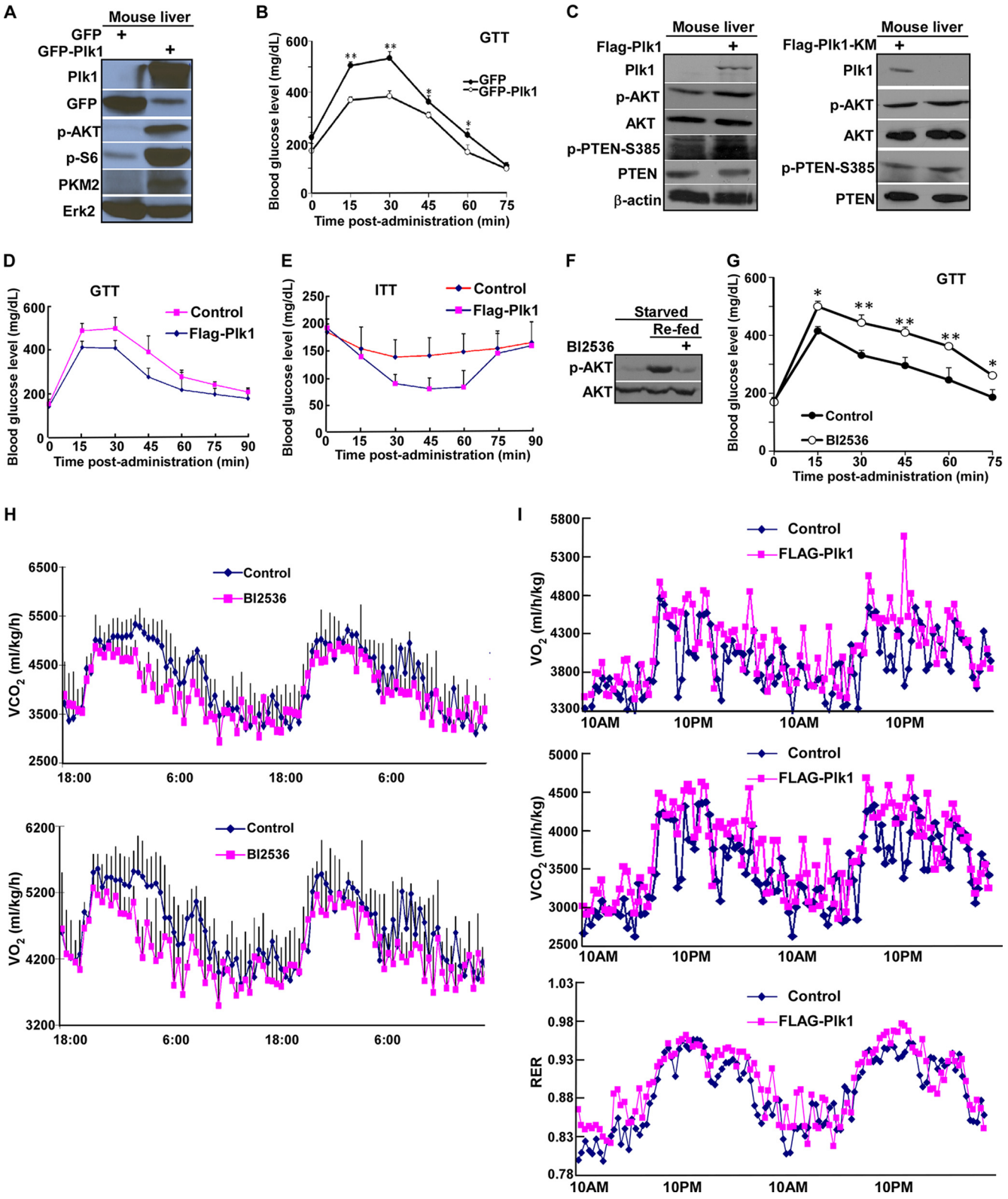

FIG 3 Plk1 regulates energy metabolism. (A and B) Adenovirus-mediated Plk1 overexpression results in activation of the PI3K pathway and increased glucose uptake. Mice were intravenously injected with adenovirus expressing Plk1. Four days later, the mice were subjected to starvation for 16 h, injected with glucose, and followed by measurement of blood glucose levels (B) and IB of liver homogenates (A). (C to E) Vector-based Plk1 overexpression causes activation of the PI3K pathway and increased glucose uptake. Male mice fed with regular chow ($n = 8$) were intravenously injected with Flag-Plk1 (WT or K82M) and either sacrificed for IB of liver homogenates (C) or subjected to GTT (D) and ITT (E). (F to H) Inhibition of Plk1 affects energy metabolism. Mice were treated with BI2536 (6 mg/kg of body weight) for 1 week, subjected to starvation for 16 h, refed, and subjected to IB of liver homogenates (F), GTT (G), and indirect calorimetry of BI2536-injected mice (BI2536) and control mice (H). Carbon dioxide release (VCO_2) and oxygen consumption (VO_2) per kg of body weight were determined in metabolic chambers ($n = 6$ per group). (I) Flag-Plk1 overexpression increases energy expenditure in mice. Male mice fed with regular chow were intravenously injected with Flag-Plk1 and subjected to indirect calorimetry within 4 days of injection. Oxygen consumption, carbon dioxide release, and RER (VCO_2/VO_2) were determined in control and Flag-Plk1-expressing mice in metabolic chambers ($n = 6$ per group). The data are presented as means and SD. *, $P < 0.05$; **, $P < 0.01$.

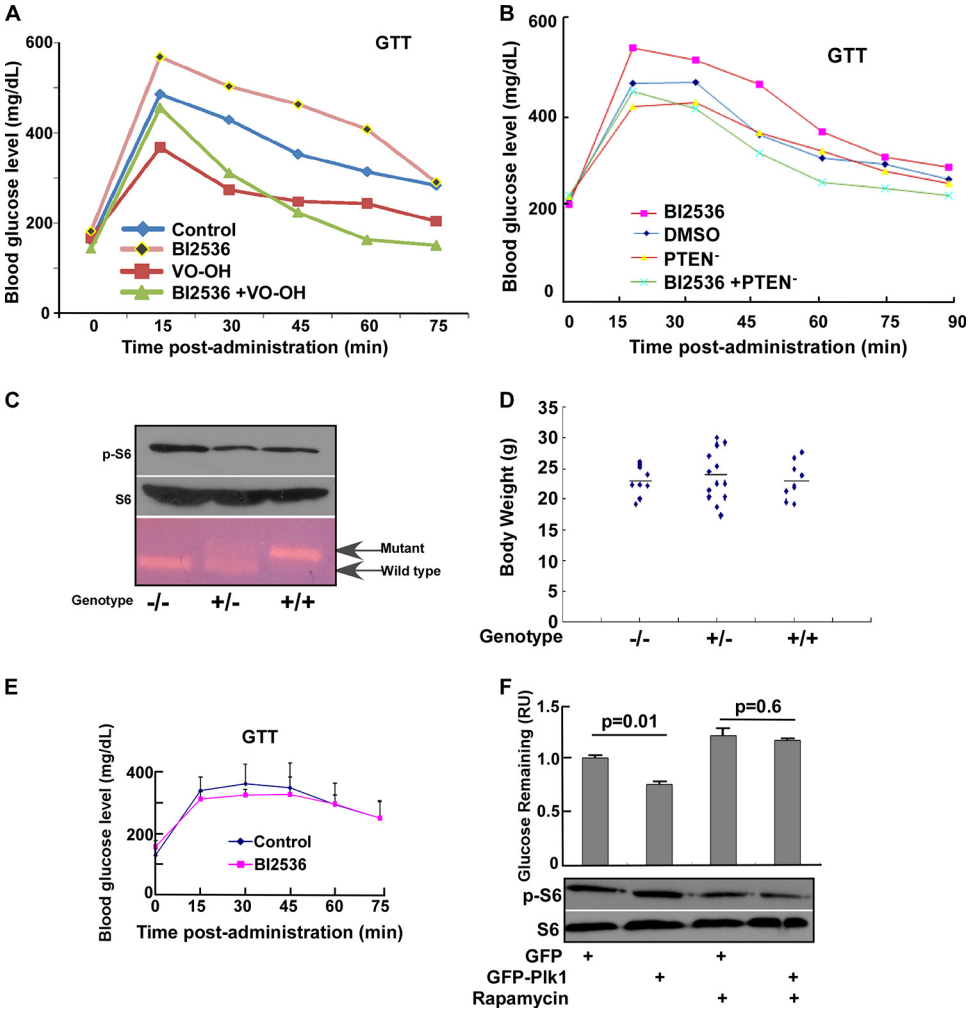

FIG 4 Plk1 regulates energy metabolism via the PTEN pathway. (A) BI2536-mediated inhibition of glucose uptake can be reversed by inhibition of PTEN. Mice were intraperitoneally injected with BI2536, VO-OH (5 μg/kg of body weight), or both drugs once a day for seven consecutive days and subjected to GTT. (B) BI2536-mediated inhibition of glucose uptake can be reversed by depletion of PTEN. Mice (WT or PTEN knockout) were intraperitoneally injected with BI2536 once a day for seven consecutive days. (C) Mice with liver-specific mTOR knockout. Liver-specific mTOR knockout mice were obtained by crossing LoxP-Stop-LoxP (LSL)-mTOR mice with mice expressing liver-specific Cre. Livers were obtained from WT, $mTOR^{+/-}$, or $mTOR^{-/-}$ mice, and total protein lysates were probed with antibodies against pS6 and S6. To test the genotypes of mTOR-depleted mice, genomic DNA was prepared from tail clips 0.5 to 0.8 mm in length and subjected to PCR. For the standard PCR, 10 ng genomic DNA was amplified using the sense primer 5′-TTA TGT TTG ATA ATT GCA GTT TTG GCT AGC AGT-3′ and the antisense primer 5′-TTT AGG ACT CCT TCT GTG ACA TAC ATT TCC T-3′. (D) Liver-specific mTOR depletion does not affect body weight in mice at the age of 6 weeks. (E) mTOR is required for Plk1-mediated regulation of energy metabolism. Liver-specific mTOR knockout mice were treated with BI2536 for 1 week and subjected to GTT. (F) Inhibition of mTORC1 reverses Plk1 overexpression-induced glucose uptake. 293T cells were transfected with Plk1 for 24 h, treated with 100 nM rapamycin for 24 h or left untreated, and harvested for measurement of the glucose remaining in the culture media (top) or for IB (bottom). The data are presented as means and SD.

constitutively active; K82M, kinase defective). As indicated, cotransfection of Plk1-T210D inhibited polyubiquitination of WT PTEN but not of PTEN-S385A, whereas cotransfection of Plk1-K82M enhanced polyubiquitination of PTEN (Fig. 6H to J), supporting the notion that Plk1 phosphorylation of PTEN-S385 inhibits its polyubiquitination and thus its degradation.

It has been established that stabilized PTEN is less active due to lack of interaction with its partners (8, 9). In agreement with this, expression of PTEN-S385A resulted in stronger inhibition of the PI3K pathway than expression of PTEN-S385D. Moreover, expression of PTEN-S385A increased cell death, as indicated by a higher level of cleaved PARP (c-PARP) and a reduced level of PKM2, suggesting that PTEN-S385A has a stronger tumor-suppressive function than PTEN-S385D (Fig. 6K). In agreement with this, cells expressing PTEN-S385A proliferated more slowly than cells expressing PTEN-S385D (Fig. 6L). Upon expression of WT PTEN and PTEN-S385A, the cells rounded up, began to detach from the culture dish within 2 days, and formed clusters in later stages. In contrast, expression of PTEN-S385D did not change the morphology significantly (Fig. 6L). Finally, ectopic expression of PTEN-S385A in 293T cells also showed a much stronger inhibitory effect on colony formation than PTEN-S385D in both anchorage-dependent (Fig. 6M) and -independent (Fig. 6N) assays.

Plk1 phosphorylation of PTEN inhibits its monoubiquitination and nuclear localization. Considering that nuclear localization of PTEN is critical for its tumor-suppressive functions, we

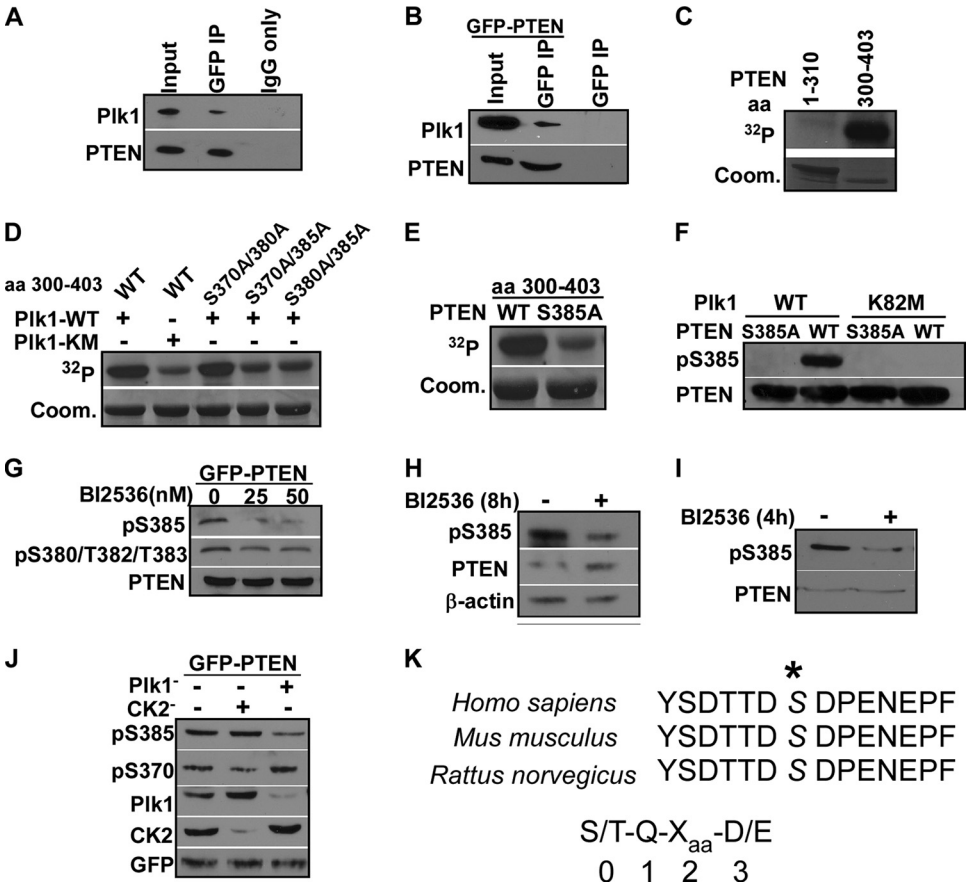

FIG 5 Plk1 phosphorylates PTEN-S385. (A) Plk1 binds to PTEN. 293T cells were cotransfected with GFP-PTEN and Flag-Plk1 and harvested for anti-GFP IP, followed by IB. (B) Cells were prepared as for panel A, but GFP IP was used as a control for nontransfected cells. (C) Plk1 phosphorylates PTEN *in vitro*. After purified Plk1 was incubated with purified GST-PTEN regions in the presence of [γ-^{32}P]ATP, the reaction mixtures were resolved by SDS-PAGE, stained with Coomassie brilliant blue (Coom.), and detected by autoradiography. aa, amino acids. (D and E) Plk1 targets PTEN-S385. Plk1 was incubated with various GST-PTEN mutants as for panel C. (F) The pS385-PTEN antibody is specific. Plk1 (WT or K82M) was incubated with GST-PTEN (WT or S385A) in the presence of unlabeled ATP, followed by anti-pS385-PTEN IB. (G) PTEN-S385 is phosphorylated *in vivo* in a Plk1 activity-dependent manner. 293T cells were transfected with PTEN and treated with BI2536 for 8 h. (H and I) Inhibition of Plk1 downregulates the phosphorylation level of endogenous PTEN at S385. 293T cells were treated with 50 nM BI2536 for 8 h (H) or 4 h (I) in the presence of 50 nM nocodazole. (J) Plk1, but not CK2, is responsible for PTEN-S385 phosphorylation *in vivo*. 293T cells were cotransfected with GFP-PTEN and pBS/U6-Plk1 to deplete Plk1 or pKD-CK2 to deplete CK2 (45). (K) Sequence context of PTEN-S385 of various species. Asterisk, phosphorylation site.

asked whether Plk1-associated kinase activity regulates the nuclear/cytoplasmic shuttling of PTEN. As indicated, inhibition of Plk1 by BI2536 completely blocked nuclear export of PTEN in DU145 (Fig. 7A and B) and RWPE1 (Fig. 7C) cells. Furthermore, BI2536 treatment also increased the nuclear PTEN signal assessed by antibodies against pS380 and pS380/pT382/pT383 of PTEN (Fig. 7D and E). We understand that inhibition of Plk1 results in mitotic arrest, which might be responsible for the increased PTEN nuclear localization. However, nocodazole treatment did not increase nuclear localization of PTEN, suggesting that the BI2536-induced increase of nuclear PTEN is not due to cell cycle arrest. To confirm this observation, we compared the subcellular localization of different PTEN constructs. The S370A mutant had a distribution pattern similar to that of WT PTEN, indicating that CK2 is unlikely to regulate the nuclear functions of PTEN. Although the S380A mutation did increase the nuclear import of PTEN, phosphorylation of S385 was clearly the most dominant factor that controlled the nuclear/cytoplasmic shuttling of PTEN, as the S385A mutant was exclusively nuclear (Fig. 7F and G). Of note, S385 was previously identified as the major phosphorylation site *in vivo* (7). In addition, PTEN nuclear localization was not affected by treatment of the cells with a CK2 inhibitor, further indicating that CK2 is not responsible for S385 phosphorylation. Finally, subcellular fractionation followed by IB confirmed the data based on IF staining (Fig. 7H).

Because monoubiquitination of PTEN leads to its nuclear import (12) and because Plk1 phosphorylation of PTEN-S385 results in its cytoplasmic accumulation, we asked whether Plk1 phosphorylation of PTEN-S385 affects its monoubiquitination. To detect monoubiquitinated PTEN, lysine-free ubiquitin (KØ-HA-Ub) was used to prevent polyubiquitin chain formation. As indicated, coexpression of constitutively active Plk1-T210D reduced the mono-ubiquitinated form of WT PTEN but not PTEN-S385A (Fig. 7I), suggesting that Plk1 phosphorylation of PTEN-S385 does inhibit its monoubiquitination. Because nuclear import of PTEN is Nedd4-1 dependent, we asked whether Plk1 phosphorylation of PTEN affects its interaction with Nedd4-1. As indicated, GFP-PTEN-S385D showed significantly reduced ability to bind

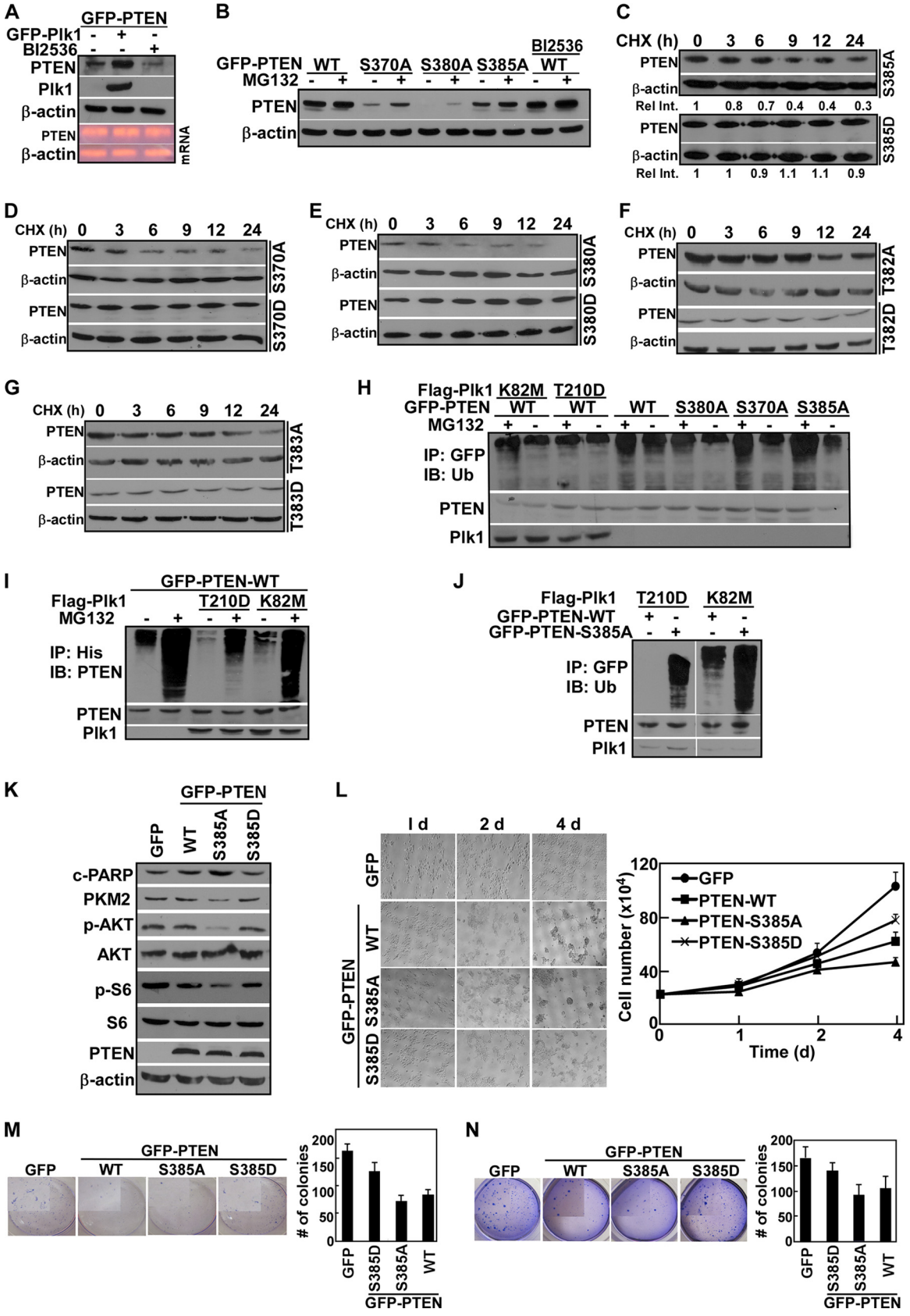

Flag-Nedd4-1 in comparison to WT PTEN and the PTEN-S385A mutant (Fig. 7J), suggesting that Plk1 phosphorylation of PTEN inhibits its interaction with Nedd4-1.

Overexpression of PTEN-S385A induces a tumor-suppressive metabolic state by regulating phosphatase-dependent and -independent pathways. Because Plk1 overexpression promotes the Warburg effect (Fig. 2), we next tested whether Plk1 phosphorylation of PTEN affects energy metabolism, in which PTEN has an established role (30). PKM2, a downstream target of the Pl3K/AKT/mTOR pathway, is a central component in cancer metabolism. As described above, expression of PTEN-S385A resulted in a reduced level of PKM2, likely due to an inactive PI3K pathway in these cells (Fig. 6K).

Because PTEN-S385A localizes mainly to the nucleus, and because nuclear PTEN is essential for the function of APC/C-Cdh1, we asked whether APC/C-Cdh1 activity is regulated by Plk1 phosphorylation of PTEN. Ectopic expression of PTEN-S385A but not WT PTEN or PTEN-S385D strongly inhibited the expression levels of cyclin B, Plk1, GLS, and PFKFB3 (Fig. 8A), four substrates of APC/C-Cdh1 (30–32). PFKFB3 catalyzes the formation of fructose 2,6-bisphosphate, which in turn activates 6-phosphofucto-1-kinase, a rate-limiting enzyme in glycolysis, whereas GLS, the first enzyme in the glutaminolysis pathway, converts glutamine to glutamate. Because nuclear PTEN regulates APC/C-Cdh1 function in a phosphatase-independent manner (11), we next asked whether the phosphatase activity of PTEN affects regulation of APC/C-Cdh1 function via the phosphorylation state at S385. As predicted, cells expressing PTEN-S385A/C124S, a phosphatase-dead mutant, behaved almost identically to cells expressing PTEN-S385A in terms of expression levels of cyclin B, GLS, and PFKFB3 (Fig. 8B and C), indicating that Plk1 phosphorylation of PTEN regulates APC/C-Cdh1 activity in a phosphatase-independent manner.

Moreover, we directly measured the levels of glucose, lactate, and glutamine in media from cells expressing different PTEN constructs. In agreement with the reduced protein levels of PKM2, PFKFB3, and GLS, cells expressing PTEN-S385A showed decreased glucose uptake (Fig. 8D), reduced lactate production (Fig. 8E), and decreased glutamine uptake (Fig. 8F). In comparison to cells expressing PTEN-S385A, cells expressing PTEN-S385A/C124S consumed more glucose and produced more lactate, suggesting that Plk1 phosphorylation of PTEN affects energy metabolism by regulating PI3K-dependent and -independent pathways. Finally, introduction of the S385A mutation in PTEN increased its ability to inhibit colony formation in both WT and C124S backgrounds (Fig. 8G and H), confirming that Plk1 phosphorylation of PTEN regulates its tumor-suppressive functions via both phosphatase-dependent and -independent pathways.

PTEN is the major mediator of Plk1 elevation-induced phenotypes. To confirm that PTEN is indeed the major mediator of deregulation of glucose metabolism and the PI3K pathway due to Plk1 elevation, we performed a series of rescue experiments. First, we showed that coexpression of PTEN-S385A significantly inhibited overexpression of Plk1-induced elevation of glucose consumption (Fig. 9A) and lactate production (Fig. 9B) and increased levels of pAKT, pS6, and PKM2 (Fig. 9C). Further, cotransfection of PTEN-S385A also antagonized Plk1-T210D expression-induced elevation of pS6 (Fig. 9D). In contrast to Plk1-T210D, expression of Plk1-K82M resulted in decreased levels of pAKT and pS6, due to a dominant-negative effect (Fig. 9D to F). Second, we showed that the PTEN inhibitor VO-OH, but not the PI3K inhibitor wortmannin, rescued the BI2536-induced decrease of pAKT (Fig. 9G). Finally, coexpression of PTEN-S385D but not WT PTEN rescued Plk1-K82M-induced inhibition of AKT activation (Fig. 9H). Therefore, we conclude that PTEN is the major mediator of the Plk1 elevation-associated Warburg effect and activation of the PI3K pathway.

Plk1 phosphorylation of Nedd4-1 also contributes to PTEN inactivation. We understand that PTEN regulation is exceedingly complex (33). Three E3 ubiquitin ligases, Nedd4-1, WWP2, and RFP, have been reported to mediate PTEN ubiquitination (34–36). We therefore tested the possibility that Plk1 also affects PTEN function via its activity toward these E3 ligases. As indicated, Plk1 also directly phosphorylates Nedd4-1 (Fig. 10A) at S328 (Fig. 10B). With a phosphospecific antibody we generated (Fig. 10C), we next showed that Nedd4-1-S328 is phosphorylated *in vivo* (Fig. 10D). Moreover, we showed that endogenous Nedd4-1 is phosphorylated at S328 in a Plk1-dependent manner (Fig. 10E). Because the activity and level of Plk1 are cell cycle regulated and because Plk1 phosphorylates Nedd4-1, we asked whether Nedd4-1 phosphorylation at S328 is regulated through the cell cycle. We analyzed phosphorylation of Nedd4-1 using pS328 antibodies in cells synchronized at various cell cycle stages. HeLa cells were synchronized with the double thymidine block (DTB) at the G_1/S boundary and released for different times. Fluorescence-activated cell sorting (FACS) was used to monitor cell cycle progression (Fig. 10F). Immunoblotting using an antibody that recognizes Nedd4-1 irrespective of its phosphorylation state indicated that the total amount of Nedd4-1 did not change during the cell cycle (Fig. 10G). However, the Nedd4-1-S328 phosphorylation level gradually increased from S phase and peaked from 12

FIG 6 Plk1 phosphorylation of PTEN-S385 inhibits its polyubiquitination, degradation, and phosphatase activity. (A) Plk1 increases the stability of PTEN. 293T cells were transfected with the indicated plasmids, treated with 50 nM BI2536 for 8 h or left untreated, and harvested for IB (top three rows) or mRNA preparation, followed by RT-PCR (bottom two rows). (B) Unphosphorylatable PTEN mutants are less stable. 293T cells were transfected with PTEN constructs and treated with 10 μM MG132 with or without BI2536 for 8 h. (C) PTEN-S385D is more stable than PTEN-S385A. 293T cells were transfected with PTEN constructs and treated with 10 μg/ml CHX for different times. (D to G) Protein degradation of PTEN with various mutations at other C-terminal phosphorylation sites. 293T cells were transfected with GFP-PTEN constructs (S370A, S370D, S380A, S380D, T382A, T382D, T383A, and T383D), treated with 10 μg/ml CHX for different times, and harvested for IB. (H to J) Plk1 inhibits polyubiquitination of PTEN. (H) 293T cells were cotransfected with His-ubiquitin and the indicated plasmids, treated with 10 μM MG132 for 12 h, and harvested for anti-GFP IP, followed by antiubiquitin IB. (I) 293T cells were cotransfected with His-ubiquitin with the indicated plasmids, treated with 10 μM MG132, and harvested for anti-His IP. (J) 293T cells were cotransfected with His-ubiquitin and the indicated plasmids, treated with 10 μM MG132, and harvested for anti-GFP IP. (K) Phosphorylation of PTEN-S385 inhibits its phosphatase activity. 293T cells were transfected with PTEN constructs for 36 h. (L to N) Phosphorylation of PTEN-S385 promotes cell proliferation and colony formation. (L) 293T cells were transfected with PTEN constructs and harvested at different times for examination of morphological change and determination of cell number. (M) 293T cells (3×10^2) expressing PTEN constructs were seeded in plates for 4 days (d), and viable colonies were counted. (N) 293T cells (2×10^3) expressing PTEN constructs were seeded in plates containing soft agar for 7 days, and viable colonies were counted. The data are presented as means and SD.

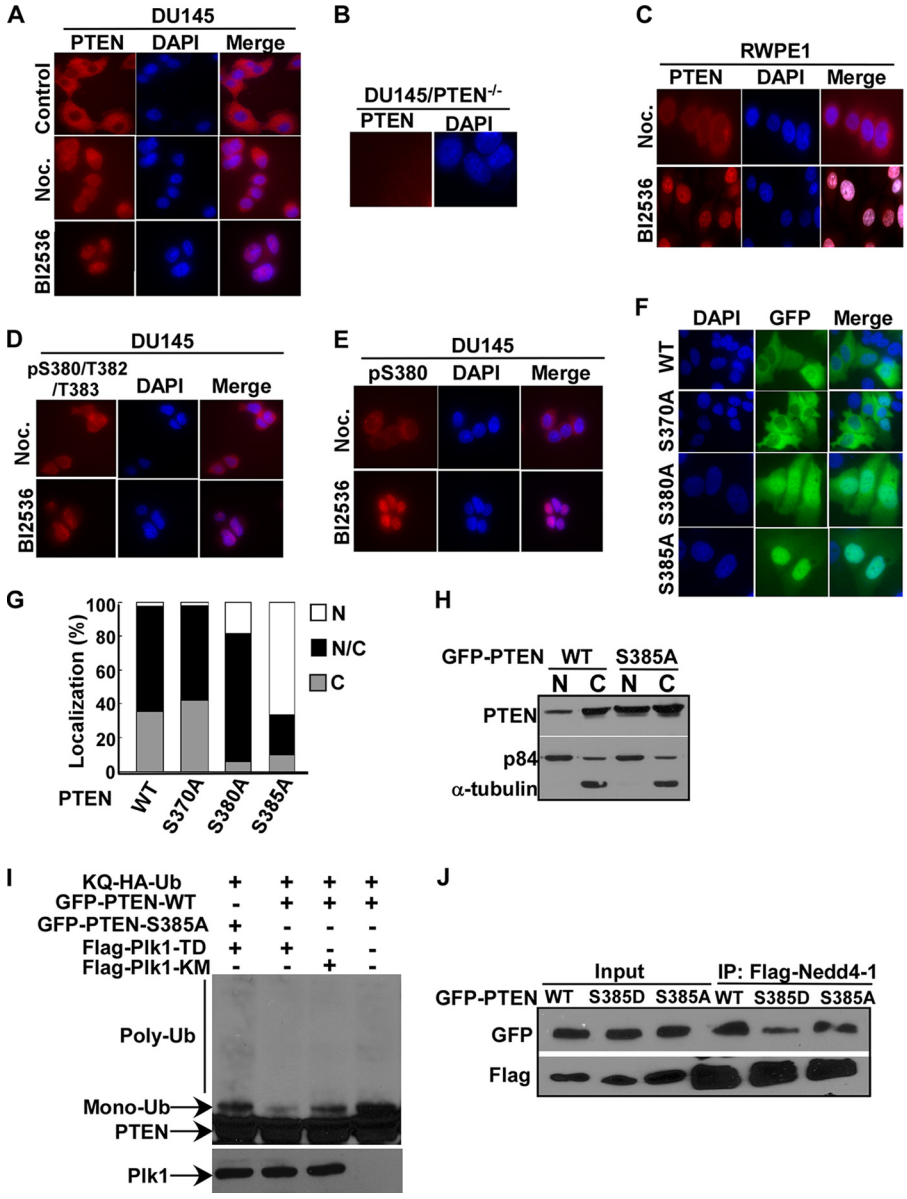

FIG 7 Plk1 inhibits nuclear localization of PTEN. (A to E) Inhibition of Plk1 increased nuclear localization of PTEN. (A) DU145 cells were treated with BI2536 or nocodazole (Noc.) for 6 h and harvested for anti-PTEN immunofluorescence (IF) staining. (B) DU145 cells were depleted of PTEN. (C to E) RWPE1 (C) or DU145 (D and E) cells were treated with nocodazole or BI2536 and subjected to IF staining with antibodies against PTEN (C), pS380/T382/T383-PTEN (D), or pS380-PTEN (E). (F to H) PTEN-S385A is exclusively nuclear. (F) PC3 cells were transfected with GFP-PTEN constructs. (G) To quantify subcellular localization of GFP-PTEN, cells were grouped as nuclear only (N), both nuclear and cytoplasmic (N/C), and cytoplasmic only (C). (H) Lysates from PC3 cells expressing different forms of PTEN were subjected to nuclear (N) and cytoplasmic (C) fractionation. (I) Plk1 phosphorylation of PTEN inhibits its monoubiquitination. 293T cells were cotransfected with the indicated plasmids and harvested for antiubiquitin IB. (J) PTEN-S385D has reduced ability to bind Nedd4-1. 293T cells were transfected with GFP-PTEN (WT, S385D, or S385A) and Flag-Nedd4-1 and harvested for anti-Flag IP, followed by anti-GFP IB.

h to 15 h as cells went through mitosis, which correlates with the Plk1 expression profile (Fig. 10G). Quantification of the results obtained in HeLa cells, using standardization with known amounts of phosphorylated and nonphosphorylated Nedd4-1, indicated that phosphorylation was increased up to 37-fold. However, as the DTB protocol did not arrest all cells and cells were not at precisely the same point, we consider this number to be an underestimate of the maximal level of phosphorylation. Thus, the degree of synchrony of the various cell preparations influenced the increase in phosphorylation observed. Furthermore, we showed that Plk1 and pS328-Nedd4-1 epitopes were colocalized in various mitotic structures, such as kinetochores in prophase, spindle poles in metaphase, midzones in telophase, and midbodies in cytokinesis (Fig. 10H to J).

We then tested the possibility that Plk1 phosphorylation of Nedd4-1 affects its E3 ubiquitin ligase activity toward PTEN. For that purpose, 293T cells were cotransfected with GFP-tagged PTEN and His-ubiquitin in the presence or absence of HA-Nedd4-1 coexpression. Next, GFP-PTEN proteins were immunoprecipitated from total cell extracts, and covalently linked His-Ub

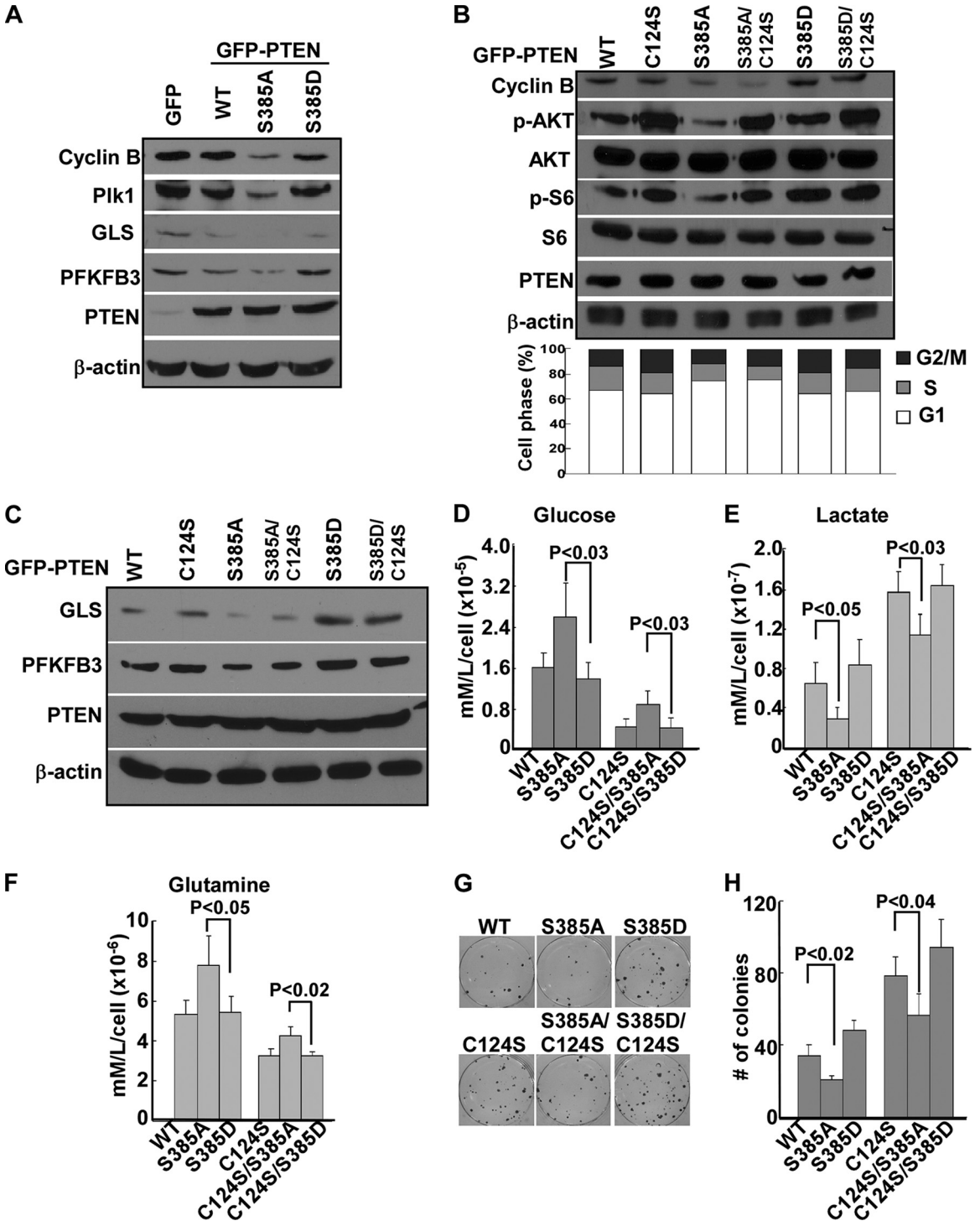

FIG 8 Plk1 phosphorylation of PTEN induces a tumor-promoting metabolic state. (A) Phosphorylation of PTEN-S385 inhibits APC/C-Cdh1 activity. 293T cells were transfected with PTEN constructs for 48 h. (B) The nuclear PTEN function is inhibited by S385 phosphorylation in a phosphatase-independent manner. PC3 cells were transfected with PTEN constructs and harvested for IB (top) or FACS analysis (bottom). (C to F) Phosphorylation of PTEN-S385 induces a tumor-promoting metabolic state. MEFs were transfected with different PTEN constructs and harvested for IB (C) or measurement of glucose (D), lactate (E), and glutamine (F) levels in the medium. (G and H) The tumor-suppressive function of PTEN is inhibited by S385 phosphorylation in both phosphatase-dependent and -independent manners. PC3 cells expressing PTEN were seeded in a six-well dish (1×10^3 cells), cultured in medium containing soft agar for 10 days, and stained with crystal violet (G), and the colonies were counted (H). The data are presented as means and SD.

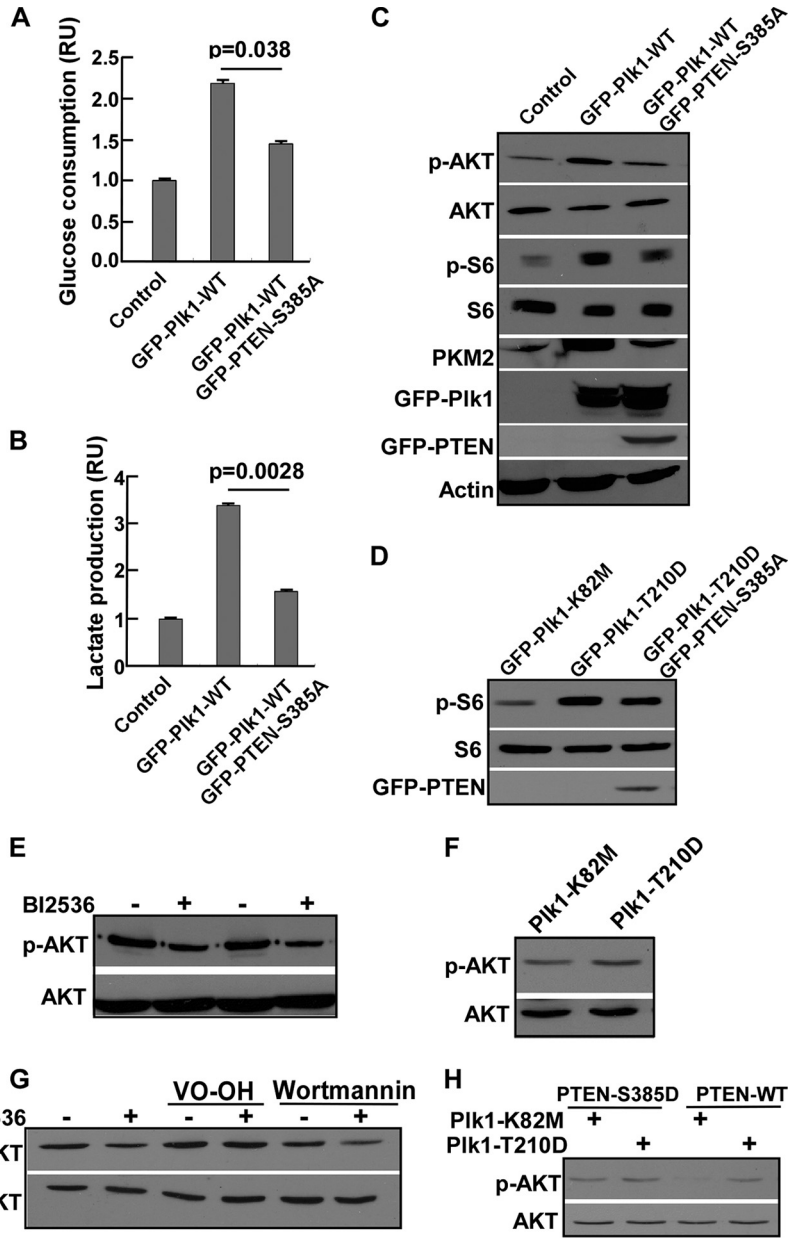

FIG 9 PTEN is the major mediator of the Plk1 elevation-associated Warburg effect and activation of the PI3K pathway. (A and B) Coexpression of PTEN-S385A rescues Plk1 overexpression-induced increased glucose uptake. After 293T cells were transfected with the indicated plasmids for 48 h, culture media were collected for measurement of glucose consumption (A) and lactate production (B). (C and D) Coexpression of PTEN-S385A rescues Plk1 overexpression-induced activation of the PI3K pathway. (C) 293T cells were transfected with the indicated plasmids for 48 h. (D) 293T cells were transfected with the indicated plasmids. (E) Inhibition of Plk1 reduces the phosphorylation level of AKT. 293T cells were treated with 50 nM BI2536 for 12 h. (F) AKT activation is regulated by Plk1 activity. 293T cells were transfected with different forms of Plk1 for 48 h. (G) Plk1-mediated activation of AKT is dependent on PTEN. 293T cells were treated with the indicated drugs for 12 h. (H) Inhibition of Plk1-associated inactivation of AKT can be rescued by overexpression of PTEN-S385D. 293T cells were cotransfected with the indicated plasmids for 48 h. The data are presented as means and SD.

was detected by immunoblotting using an anti-His antibody. As shown in Fig. 10K, the patterns and intensities of bands recognized by the anti-His antibodies were comparable in cells with or without Nedd4-1, indicating that overexpression of Nedd4-1 does not significantly affect the ubiquitination of WT PTEN. Next, we asked whether Plk1-mediated phosphorylation of Nedd4-1 regulates its activity toward PTEN. Accordingly, 293T cells were cotransfected with GFP-PTEN, His-ubiquitin, and various HA-Nedd4-1 (WT, S328A, or S328D) constructs. Our results showed that Plk1-mediated phosphorylation of Nedd4-1 was unable to stimulate or inhibit WT-PTEN ubiquitination (Fig. 10L). Pulse-chase experiments performed with cycloheximide (CHX) to block protein synthesis also revealed no difference in PTEN stability (Fig. 10M and N). Thus, our results suggest that Nedd4-1 or Plk1 phosphorylation of Nedd4-1 had no significant effect on the stability or ubiquitination of wild-type PTEN.

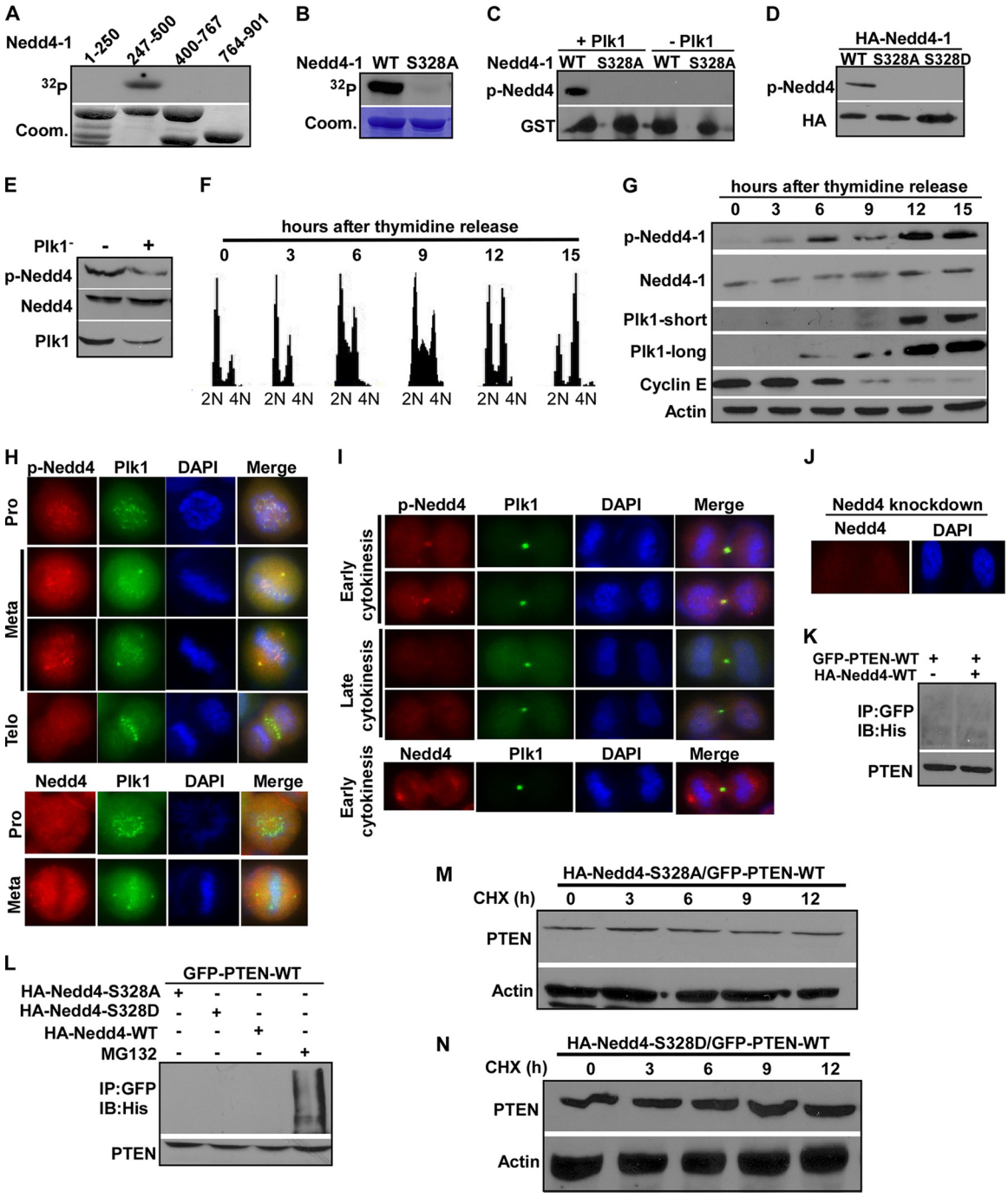

FIG 10 Plk1 targets Nedd4-1 at S328. (A and B) Plk1 phosphorylates Nedd4-1-S328. Plk1 was incubated with GST-Nedd4-1 regions (A) or different mutants (B) as for Fig. 3B. (C) The pS328-Nedd4-1 antibody is specific. Plk1 was incubated with GST-Nedd4-1 in the presence of unlabeled ATP. (D) Nedd4-1-S328 is phosphorylated *in vivo*. 293T cells were transfected with Nedd4-1 constructs for 48 h. (E) Endogenous Plk1 phosphorylates endogenous Nedd4-1 at S328. 293T cells were depleted of Plk1 by RNAi for 48 h. (F and G) Phosphorylation of Nedd4-1-S328 is cell cycle regulated. HeLa cells were subjected to a double thymidine block (16 h of thymidine treatment, 8 h of release, and a second thymidine block for 16 h), released for different times, and harvested for FACS analysis (F) or IB (G). (H to J) Colocalization of pNedd4-1 and Plk1 at mitotic structures. HeLa cells were subjected to IF staining with the indicated antibodies. Pro, prophase; Meta, metaphase; Telo, telophase. (K to N) Phosphorylation of Nedd4-1-S328 does not affect its E3 ubiquitin ligase activity toward WT-PTEN. (K) 293T cells were cotransfected with GFP-PTEN, HA-Nedd4-1, and His-ubiquitin and harvested for anti-GFP IP, followed by anti-His IB. (L) 293T cells were cotransfected with the indicated plasmids, treated with MG132 or left untreated, and harvested for anti-GFP IP, followed by anti-His IB. (M and N) 293T cells were cotransfected with the indicated plasmids, treated with cycloheximide for different times, and harvested for IB.

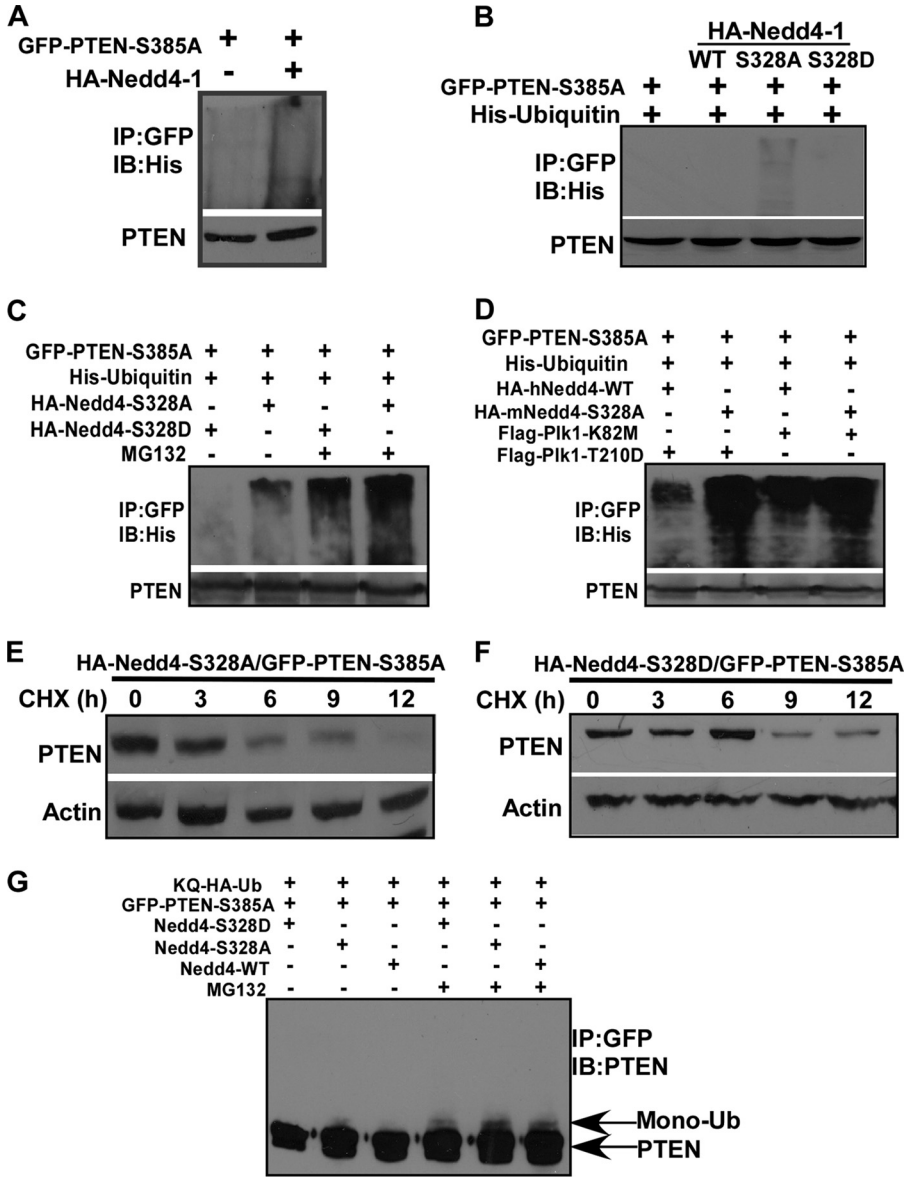

FIG 11 Plk1 phosphorylation of Nedd4-1-S328 inhibits its E3 ubiquitin ligase activity toward PTEN-S385A. (A) 293T cells were cotransfected with His-ubiquitin and the indicated plasmids and harvested for anti-GFP IP, followed by anti-His IB. (B) 293T cells were cotransfected with the indicated plasmids and harvested for anti-GFP IP. (C) 293T cells were cotransfected with the indicated plasmids for 36 h, treated with MG132 for 6 h or left untreated, and harvested for anti-GFP IP. (D) 293T cells were cotransfected with the indicated plasmids, treated with MG132 for 6 h, and harvested for anti-GFP IP. (E and F) 293T cells were cotransfected with the indicated plasmids, treated with cycloheximide for the indicated times, and harvested. (G) Phosphorylation of Nedd4-1-S328 inhibits its monoubiquitination activity toward PTEN-S385A. 293T cells were cotransfected with the indicated plasmids for 36 h, treated with MG132 for 6 h or left untreated, and harvested for anti-GFP IP.

Considering that phosphorylation of PTEN-S385 plays a crucial role in regulating PTEN ubiquitination and degradation, we further asked whether Plk1 phosphorylation of Nedd4-1 might have a role in the regulation of PTEN-S385A. 293T cells were cotransfected with GFP-PTEN-S385A and His-ubiquitin with or without HA-Nedd4-1. As indicated, overexpression of Nedd4-1 in 293T cells indeed caused an increase of PTEN-S385A ubiquitination (Fig. 11A). More significantly, cells expressing Nedd4-1-S328A exhibited a higher level of PTEN-S385A polyubiquitination than cells expressing Nedd4-1-S328D (Fig. 11B), which could be further amplified by MG132 (Fig. 11C), indicating that Nedd4-1-S328 phosphorylation prevents PTEN-S385A polyubiquitination. Further, Nedd4-1-expressing cells with coexpression of Plk1-K82M had a higher level of polyubiquitination of PTEN than those with coexpression of Plk1-T210D, but such a difference was minimized in Nedd4-1-S328A-expressing cells, suggesting that Plk1 phosphorylation of Nedd4-1-S328 contributes to PTEN polyubiquitination (Fig. 11D). In agreement with this, pulse-chase experiments revealed that cells expressing Nedd4-1-S328A exhibited a much shorter half-life of PTEN-S385A than cells expressing Nedd4-1-S328D (Fig. 11E and F), further indicating that Nedd4-1-S328 phosphorylation prevents PTEN-S385A polyubiq-

uitination and degradation. Finally, we showed that Nedd4-1-S328 phosphorylation also inhibits PTEN-S385A monoubiquitination (Fig. 11G). Therefore, Plk1 phosphorylation of Nedd4-1 inhibits its E3 ligase activity toward PTEN in a specific cellular context.

Plk1 phosphorylation of PTEN inhibits its autodephosphorylation activity. Because S385 is the major phosphorylation site (7), we asked whether Plk1 phosphorylation of PTEN-S385 affects the phosphorylation status of other sites. Cells expressing PTEN-S385A showed significantly lower phosphorylation levels at S370, S380, and S380/T382/T383 than cells expressing PTEN-S385D (Fig. 12A), suggesting that phosphorylation at S385 enhances phosphorylation at other sites. We also analyzed the potential effects of S370 and S380 on phosphorylation of S385. Introduction of the S370A (Fig. 12B) or S380A (Fig. 12C) mutation did not significantly affect the phosphorylation level of S385. We tested two possibilities that might be responsible for the observation shown in Fig. 12A. First, we asked whether Plk1 phosphorylation of PTEN creates a docking site for other kinases, such as CK2, subsequently enhancing phosphorylation at other sites. A sequential kinase assay was performed. Prior incubation of PTEN with Plk1 did not render it a more robust substrate for CK2 (Fig. 12D and E), indicating that Plk1 phosphorylation of PTEN-S385 did not affect phosphorylation of PTEN by CK2. In support of this, the GST-PTEN-S385D mutant was not more susceptible to CK2 phosphorylation (Fig. 12D, lane 5). Second, we asked whether S385 phosphorylation inhibits the autodephosphorylation activity of PTEN, as a striking feature of PTEN is its predilection for autodephosphorylation (37). For that purpose, we compared the phosphorylation levels of PTEN in cells expressing either WT PTEN or the PTEN-C124S mutant. We found that phosphorylation of S370, S380, T382, and T383 but not S385 was markedly decreased in cells expressing WT-PTEN compared to cells expressing PTEN-C124S (Fig. 12F), indicating that PTEN dephosphorylates itself at S370, S380, T382, and T383 but not at S385. Next, we compared the phosphorylation levels of other sites in cells expressing PTEN-S385A versus PTEN-S385A/C124S. Cells expressing PTEN-S385A/C124S showed higher levels of phosphorylation at S370, S380, T382, and T383 than cells expressing PTEN-S385A, suggesting that S385 phosphorylation inhibits autodephosphorylation of S370, S380, T382, and T383. In agreement with this, cells expressing both PTEN-S385D and PTEN-S385D/C124S showed high levels of phosphorylation at S370, S380, T382, and T383 (Fig. 12G).

As phosphorylation of PTEN at S385 affects the phosphorylation of the C-terminal cluster, which is critical to regulate PTEN stability, we next explored the possibility that S385 controls PTEN stability by affecting its autodephosphorylation toward other sites. To address this question, the serine/threonine cluster S380/T382/T383 was mutated to phosphomimic aspartic acid (D), while S385 was mutated to alanine (A) (S380D/T382D/T383D/S385A [3D:A]). Then, the relevant phosphorylation site mutants were produced in 293T cells by transient transfection, and the steady-state levels of GFP-PTEN (WT or mutants) were determined by immunoblot analysis. While the S385A mutation resulted in a marked decrease in the steady-state protein level, S380D/T382D/T383D (3D) and 3D:A mutations did not change the steady-state level of PTEN (Fig. 12H). Furthermore, pulse-chase experiments revealed a marked reduction in the S385A half-life. In contrast, the stability of the 3D:A mutant was almost identical to that of WT PTEN (Fig. 12I). To investigate whether the 3D:A mutation increased PTEN stability by inhibiting PTEN ubiquitination, we cotransfected His-ubiquitin and various forms of GFP-PTEN into 293T cells, followed by anti-GFP IP and anti-His IB. As expected, the more stable 3D:A mutant displayed apparently less intensity of His-ubiquitin conjugation events than the S385A mutant (Fig. 12J). On the basis of all these results, our findings strongly indicate that the reduced stability of PTEN-S385A is due to PTEN autodephosphorylation toward the C-terminal cluster.

Dephosphorylation of PTEN at the C-terminal cluster plays a role not only in reducing its protein stability but also in increasing its phosphatase activity. To determine whether the resulting increase of phosphatase activity by dephosphorylation of PTEN-S385 is due to PTEN autodephosphorylation, the effects of 3D:A, S385A, and S385D on the phosphorylation of AKT were compared. As indicated in Fig. 12K, the abilities of S385A and 3D:A to reduce pAKT were similar compared to that of S385D, suggesting that PTEN-S385A regulates its phosphatase activity independently of the autodephosphorylation of PTEN. Moreover, expression of both PTEN-S385A and PTEN-3D:A led to cell death, as indicated by higher levels of c-PARP than cells expressing PTEN-S385D (Fig. 12K), suggesting that PTEN-S385A and PTEN-3D:A likely have similar tumor-suppressive functions.

We continued to evaluate whether the S385A increase of nuclear import is due to increased autodephosphorylation of PTEN. As indicated, the S385A and 3D:A mutants equally favored PTEN nuclear accumulation, while the 3D mutant was localized in the cytoplasm (Fig. 12L). Further, subcellular fractionation followed by IB confirmed the data based on IF staining (Fig. 12M). Therefore, dephosphorylation of PTEN-S385 enhances PTEN nuclear localization in a manner independent of its autodephosphorylation. We also asked whether APC/C-Cdh1 activity is regulated by 3D:A. Ectopic expression of PTEN-S385A and 3D:A but not 385D strongly inhibited the expression levels of cyclin B and Plk1 (Fig. 12N). Finally, we showed that cells expressing PTEN-S385A and PTEN-3D:A have similar colony formation abilities (Fig. 12O). Thus, we conclude that additional phosphorylation at S380/T382/T383 did not significantly affect PTEN-S385A expression-induced phenotypes and that S385 phosphorylation has a much more dominant effect than phosphorylation of other sites in the regulation of PTEN functions.

Plk1 phosphorylation of PTEN-S385 inhibits its tumor-suppressive function in human prostate cancer xenografts. Finally, we directly compared the tumor-suppressive abilities of different forms of PTEN with a human prostate cancer xenograft model. As indicated in Fig. 13A to C, the tumors carrying PTEN-S385A were the smallest, whereas the tumors expressing PTEN-S385D/C124S had the largest volume and weight, suggesting that Plk1 phosphorylation of PTEN-S385 inhibits its tumor-suppressive function by regulating both phosphatase-dependent and -independent pathways.

DISCUSSION

It is well established that Plk1 is involved in almost every step of mitosis (14). However, increasing evidence suggests that Plk1 has additional, nonmitotic functions that might play a more critical role in tumorigenesis. Because one tends to think that overexpression of Plk1 in cancer cells is simply a secondary effect of higher proliferation, we previously compared expression levels of Plk1 in well-synchronized cells. We showed that the levels of Plk1 are

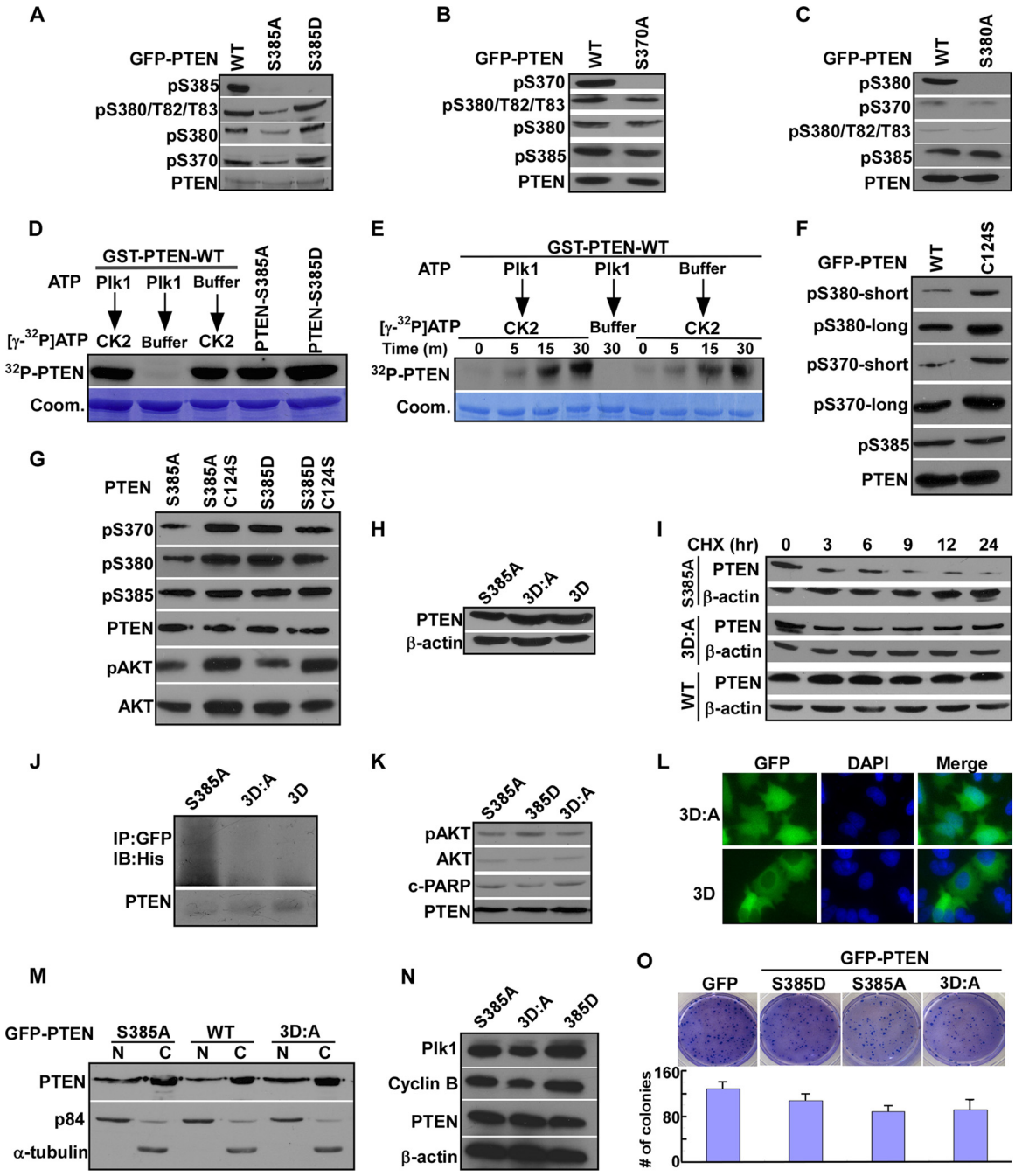

FIG 12 Plk1 phosphorylation of PTEN-S385 inhibits its autodephosphorylation of other phosphorylation sites. (A) Expression of PTEN-S385A inhibits phosphorylation levels of PTEN-S370, -S380, -T382, and -T383. 293T cells were transfected with PTEN constructs for 24 h. (B and C) Expression of PTEN-S370A and -S380A does not affect S385 phosphorylation. 293T cells were transfected with PTEN constructs for 24 h. (D and E) Prior phosphorylation of PTEN by Plk1 does not affect the subsequent phosphorylation of PTEN by CK2. (D) Different forms of purified GST-PTEN (WT, S385A, and S385D) were incubated with purified Plk1 in the presence of unlabeled ATP, followed by incubation with CK2 in the presence of [γ-^{32}P]ATP. (E) The experimental setup was the same as for panel D, but CK2 was incubated for a different time. (F) S370, S380, T382, and T383, but not S385, can be autodephosphorylated by PTEN. 293T cells were transfected with GFP-PTEN constructs (WT or C124S mutant) and harvested for IB. (G) Expression of PTEN-S385A decreases the phosphorylation levels of S370, S380, T382, and T383 in a phosphatase-dependent manner. 293T cells were transfected with PTEN constructs for 24 h. (H) Introduction of 3D mutations increases the stability of PTEN-S385A. Cells expressing the indicated forms of PTEN were subjected to IB. (I) Introduction of the 3D mutation increases the half-life of PTEN-S385A. 293T cells were transfected with PTEN constructs and treated with 10 μg/ml CHX for different times. (J) The PTEN-3D:A mutant has reduced ubiquitination. 293T cells were cotransfected with GFP-PTEN constructs and His-ubiquitin and harvested for anti-GFP IP, followed by anti-His IB. (K) S385A-associated inhibition of the PI3K pathway and increase of cell death are not affected by additional 3D mutations. 293T cells were transfected with PTEN constructs for 24 h. (L) PTEN-3D:A still localizes primarily to the nucleus. 293T cells expressing GFP-PTEN (3D or 3D:A) were stained with DAPI (4′,6-diamidino-2-phenylindole). (M) Introduction of 3D mutations does not affect S385A-associated increase of nuclear localization. 293T cells were transfected with PTEN constructs for 24 h and subjected to subcellular fractionation. (N) PTEN-S385A overexpression-associated activation of APC/C-Cdh1 activity is not affected by introduction of additional 3D mutations. 293T cells were transfected with the indicated PTEN constructs and harvested for IB. (O) Introduction of 3D mutations does not affect S385A-associated inhibition of colony formation. 293T cells expressing PTEN constructs were seeded in six-well plates (4×10^3 cells) and cultured for 7 days, and viable colonies were counted. The data are presented as means and SD.

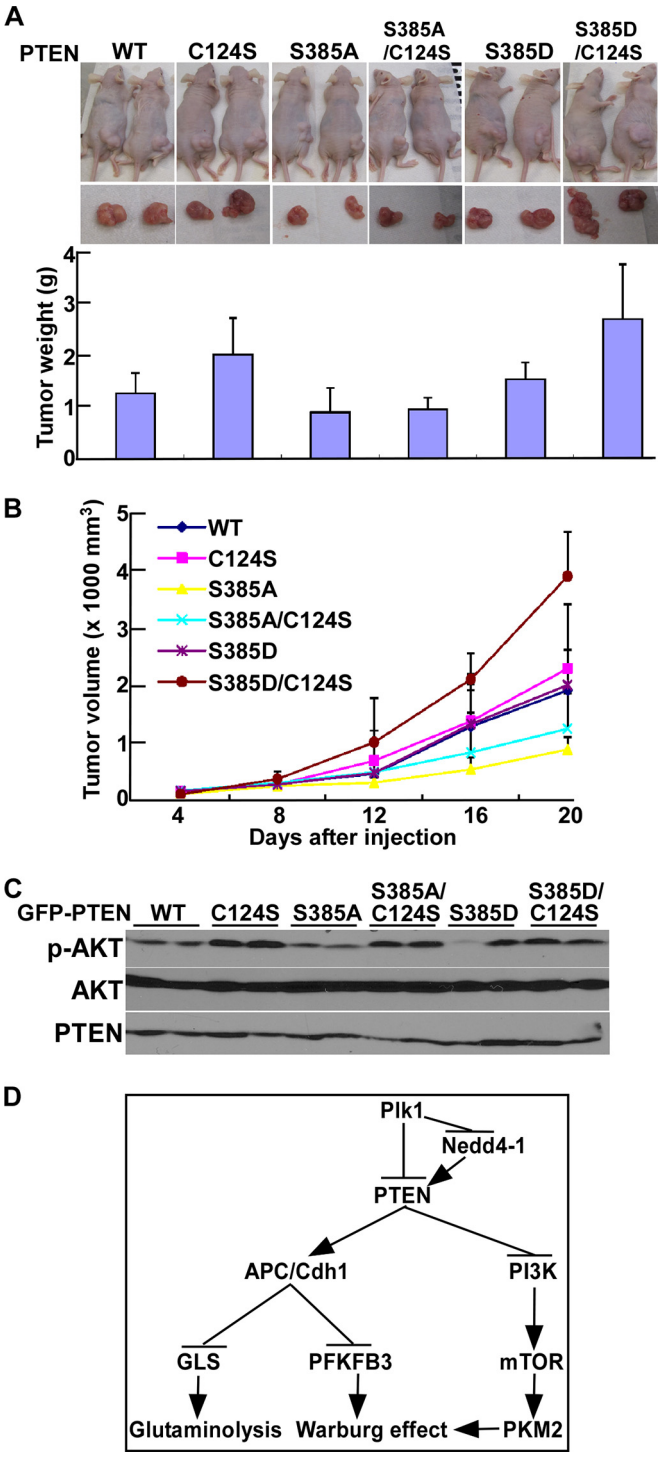

FIG 13 Plk1 phosphorylation of PTEN-S385 inhibits its tumor-suppressive function by regulating PI3K-dependent and -independent pathways. (A and B) PC3 cells were infected with retroviruses expressing PTEN constructs and injected subcutaneously into nude mice on the flank ($n = 6$ mice/group). Mice carrying tumors were followed for 3 weeks before being sacrificed. (C) IB of tumor lysates. (D) Proposed working model. The data are presented as means and SD.

significantly higher in cancer cells than in normal cells at the same stage of the cell cycle. Expression of Plk1 can be easily detected even in the G_1/S phase of most cancer cells but not in nontransformed cells. Furthermore, Plk1 localizes mainly to the nucleus in the interphase of cancer cells (38), suggesting that Plk1 must have cancer cell-specific functions in interphase. In agreement with this, depletion of Plk1 with RNAi results in both G_1 and G_2 arrest (39). Such an observation was later confirmed by the fact that Plk1 is involved in DNA replication in cancer cells (40–42). Of note, the nuclear localization of Plk1 in the interphase of cancer cells has been independently confirmed by others (43).

Here, using an adenovirus-based approach, we have shown that overexpression of Plk1 results in the Warburg effect in several different nontransformed cell lines, indicating that this observation is unlikely to be cell line specific. Considering the important role of the Warburg effect in tumorigenesis, this finding provides further evidence that elevated Plk1 is not just a secondary effect of higher proliferation of cancer cells. In contrast, our data suggest that elevation of Plk1 directly contributes to cellular transformation.

To dissect the mechanism underlying Plk1-mediated deregulation of energy metabolism, we identified PTEN as its major target in this process. It was recently shown that systemic elevation of PTEN induces a tumor-suppressive metabolic state by regulating PI3K-dependent and -independent pathways (30). We provide data to show that this important function of PTEN is regulated by Plk1-associated phosphorylation of PTEN and Nedd4-1. Significantly, Plk1 phosphorylation of PTEN and Nedd4-1 inhibits PTEN ubiquitination, the major regulatory mechanism of PTEN. Prevention of polyubiquitination of PTEN results in its stabilization, albeit with less activity toward PIP3, and thus activation of the PI3K pathway and PKM2, a master regulator of glycolysis. Inhibition of monoubiquitination of PTEN results in its nuclear exclusion and inactive APC/C-Cdh1, and thus elevated levels of PFKFB3 and GLS, rate-limiting factors of glycolysis and glutaminolysis, respectively. Therefore, we provide a novel mechanism to link Plk1, PTEN, energy metabolism, and tumorigenesis (Fig. 13D). In addition, Plk1 phosphorylation of PTEN might also regulate its newly identified mitotic activity (44).

ACKNOWLEDGMENTS

We are grateful to Eleanor Erikson for critical reading of the manuscript.

This work was supported by NIH grant R01CA157429 (X.L.), NIH grant R01CA124586 (S.F.K.), NIH grant R01CA176748 (N.A.), NSF grant MCB-1049693 (X.L.), and ACS grant RSG-13-073 (X.L.). Xenograft data were acquired by a Purdue Center for Cancer Research facility supported by Purdue Center for Cancer Research grant P30 CA023168, and support for this publication was made possible by P30 CA023168.

REFERENCES

1. **Locasale JW, Cantley LC.** 2011. Metabolic flux and the regulation of mammalian cell growth. Cell Metab. **14:**443–451. http://dx.doi.org/10.1016/j.cmet.2011.07.014.
2. **Cantley LC, Neel BG.** 1999. New insights into tumor suppression: PTEN suppresses tumor formation by restraining the phosphoinositide 3-kinase/AKT pathway. Proc. Natl. Acad. Sci. U. S. A. **96:**4240–4245. http://dx.doi.org/10.1073/pnas.96.8.4240.
3. **Schmelzle T, Hall MN.** 2000. TOR, a central controller of cell growth. Cell **103:**253–262. http://dx.doi.org/10.1016/S0092-8674(00)00117-3.
4. **Maehama T, Dixon JE.** 1998. The tumor suppressor, PTEN/MMAC1, dephosphorylates the lipid second messenger, phosphatidylinositol 3,4,5-trisphosphate. J. Biol. Chem. **273:**13375–13378. http://dx.doi.org/10.1074/jbc.273.22.13375.
5. **Turban S, Stretton C, Drouin O, Green CJ, Watson ML, Gray A, Ross F, Lantier L, Viollet B, Hardie DG, Marette A, Hundal HS.** 2012. Defining the contribution of AMP-activated protein kinase (AMPK) and protein kinase C (PKC) in regulation of glucose uptake by metformin in

skeletal muscle cells. J. Biol. Chem. **287:**20088–20099. http://dx.doi.org/10.1074/jbc.M111.330746.
6. **Sun Q, Chen X, Ma J, Peng H, Wang F, Zha X, Wang Y, Jing Y, Yang H, Chen R, Chang L, Zhang Y, Goto J, Onda H, Chen T, Wang MR, Lu Y, You H, Kwiatkowski D, Zhang H.** 2011. Mammalian target of rapamycin up-regulation of pyruvate kinase isoenzyme type M2 is critical for aerobic glycolysis and tumor growth. Proc. Natl. Acad. Sci. U. S. A. **108:**4129–4134. http://dx.doi.org/10.1073/pnas.1014769108.
7. **Torres J, Pulido R.** 2001. The tumor suppressor PTEN is phosphorylated by the protein kinase CK2 at its C terminus. Implications for PTEN stability to proteasome-mediated degradation. J. Biol. Chem. **276:**993–998. http://dx.doi.org/10.1074/jbc.M009134200.
8. **Vazquez F, Grossman SR, Takahashi Y, Rokas MV, Nakamura N, Sellers WR.** 2001. Phosphorylation of the PTEN tail acts as an inhibitory switch by preventing its recruitment into a protein complex. J. Biol. Chem. **276:**48627–48630. http://dx.doi.org/10.1074/jbc.C100556200.
9. **Vazquez F, Ramaswamy S, Nakamura N, Sellers WR.** 2000. Phosphorylation of the PTEN tail regulates protein stability and function. Mol. Cell. Biol. **20:**5010–5018. http://dx.doi.org/10.1128/MCB.20.14.5010-5018.2000.
10. **Salmena L, Carracedo A, Pandolfi PP.** 2008. Tenets of PTEN tumor suppression. Cell **133:**403–414. http://dx.doi.org/10.1016/j.cell.2008.04.013.
11. **Song MS, Carracedo A, Salmena L, Song SJ, Egia A, Malumbres M, Pandolfi PP.** 2011. Nuclear PTEN regulates the APC-CDH1 tumor-suppressive complex in a phosphatase-independent manner. Cell **144:**187–199. http://dx.doi.org/10.1016/j.cell.2010.12.020.
12. **Trotman LC, Wang X, Alimonti A, Chen Z, Teruya-Feldstein J, Yang H, Pavletich NP, Carver BS, Cordon-Cardo C, Erdjument-Bromage H, Tempst P, Chi SG, Kim HJ, Misteli T, Jiang X, Pandolfi PP.** 2007. Ubiquitination regulates PTEN nuclear import and tumor suppression. Cell **128:**141–156. http://dx.doi.org/10.1016/j.cell.2006.11.040.
13. **Howitt J, Lackovic J, Low LH, Naguib A, Macintyre A, Goh CP, Callaway JK, Hammond V, Thomas T, Dixon M, Putz U, Silke J, Bartlett P, Yang B, Kumar S, Trotman LC, Tan SS.** 2012. Ndfip1 regulates nuclear Pten import in vivo to promote neuronal survival following cerebral ischemia. J. Cell Biol. **196:**29–36. http://dx.doi.org/10.1083/jcb.201105009.
14. **Strebhardt K.** 2010. Multifaceted polo-like kinases: drug targets and antitargets for cancer therapy. Nat. Rev. Drug Discov. **9:**643–660. http://dx.doi.org/10.1038/nrd3184.
15. **Degenhardt Y, Lampkin T.** 2010. Targeting Polo-like kinase in cancer therapy. Clin. Cancer Res. **16:**384–389. http://dx.doi.org/10.1158/1078-0432.CCR-09-1380.
16. **Grosstessner-Hain K, Hegemann B, Novatchkova M, Rameseder J, Joughin BA, Hudecz O, Roitinger E, Pichler P, Kraut N, Yaffe MB, Peters JM, Mechtler K.** 2011. Quantitative phospho-proteomics to investigate the polo-like kinase 1-dependent phospho-proteome. Mol. Cell. Proteomics **10:**M111.008540. http://dx.doi.org/10.1074/mcp.M111.008540.
17. **Iliuk A, Liu XS, Xue L, Liu X, Tao WA.** 2012. Chemical visualization of phosphoproteomes on membrane. Mol. Cell. Proteomics **11:**629–639. http://dx.doi.org/10.1074/mcp.O112.018010.
18. **Santamaria A, Wang B, Elowe S, Malik R, Zhang F, Bauer M, Schmidt A, Sillje HH, Korner R, Nigg EA.** 2011. The Plk1-dependent phosphoproteome of the early mitotic spindle. Mol. Cell. Proteomics **10:**M110.004457. http://dx.doi.org/10.1074/mcp.M110.004457.
19. **Lenart P, Petronczki M, Steegmaier M, Di Fiore B, Lipp JJ, Hoffmann M, Rettig WJ, Kraut N, Peters JM.** 2007. The small-molecule inhibitor BI 2536 reveals novel insights into mitotic roles of polo-like kinase 1. Curr. Biol. **17:**304–315. http://dx.doi.org/10.1016/j.cub.2006.12.046.
20. **Liu X, Lei M, Erikson RL.** 2006. Normal cells, but not cancer cells, survive severe Plk1 depletion. Mol. Cell. Biol. **26:**2093–2108. http://dx.doi.org/10.1128/MCB.26.6.2093-2108.2006.
21. **Raab M, Kappel S, Kramer A, Sanhaji M, Matthess Y, Kurunci-Csacsko E, Calzada-Wack J, Rathkolb B, Rozman J, Adler T, Busch DH, Esposito I, Fuchs H, Gailus-Durner V, Klingenspor M, Wolf E, Sanger N, Prinz F, Angelis MH, Seibler J, Yuan J, Bergmann M, Knecht R, Kreft B, Strebhardt K.** 2011. Toxicity modelling of Plk1-targeted therapies in genetically engineered mice and cultured primary mammalian cells. Nat. Commun. **2:**395. http://dx.doi.org/10.1038/ncomms1395.
22. **Ouyang H, Mou L, Luk C, Liu N, Karaskova J, Squire J, Tsao MS.** 2000. Immortal human pancreatic duct epithelial cell lines with near normal genotype and phenotype. Am. J. Pathol. **157:**1623–1631. http://dx.doi.org/10.1016/S0002-9440(10)64800-6.
23. **Roig AI, Eskiocak U, Hight SK, Kim SB, Delgado O, Souza RF, Spechler SJ, Wright WE, Shay JW.** 2010. Immortalized epithelial cells derived from human colon biopsies express stem cell markers and differentiate in vitro. Gastroenterology **138:**1012–1021. http://dx.doi.org/10.1053/j.gastro.2009.11.052.
24. **Soule HD, Maloney TM, Wolman SR, Peterson WD, Jr, Brenz R, McGrath CM, Russo J, Pauley RJ, Jones RF, Brooks SC.** 1990. Isolation and characterization of a spontaneously immortalized human breast epithelial cell line, MCF-10. Cancer Res. **50:**6075–6086.
25. **Bello D, Webber MM, Kleinman HK, Wartinger DD, Rhim JS.** 1997. Androgen responsive adult human prostatic epithelial cell lines immortalized by human papillomavirus 18. Carcinogenesis **18:**1215–1223. http://dx.doi.org/10.1093/carcin/18.6.1215.
26. **Wan L, Zou W, Gao D, Inuzuka H, Fukushima H, Berg AH, Drapp R, Shaik S, Hu D, Lester C, Eguren M, Malumbres M, Glimcher LH, Wei W.** 2011. Cdh1 regulates osteoblast function through an APC/C-independent modulation of Smurf1. Mol. Cell **44:**721–733. http://dx.doi.org/10.1016/j.molcel.2011.09.024.
27. **Zincarelli C, Soltys S, Rengo G, Rabinowitz JE.** 2008. Analysis of AAV serotypes 1–9 mediated gene expression and tropism in mice after systemic injection. Mol. Ther. **16:**1073–1080. http://dx.doi.org/10.1038/mt.2008.76.
28. **Liu F, Song Y, Liu D.** 1999. Hydrodynamics-based transfection in animals by systemic administration of plasmid DNA. Gene Ther. **6:**1258–1266. http://dx.doi.org/10.1038/sj.gt.3300947.
29. **Mak LH, Vilar R, Woscholski R.** 2010. Characterisation of the PTEN inhibitor VO-OHpic. J. Chem. Biol. **3:**157–163. http://dx.doi.org/10.1007/s12154-010-0041-7.
30. **Garcia-Cao I, Song MS, Hobbs RM, Laurent G, Giorgi C, de Boer VC, Anastasiou D, Ito K, Sasaki AT, Rameh L, Carracedo A, Vander Heiden MG, Cantley LC, Pinton P, Haigis MC, Pandolfi PP.** 2012. Systemic elevation of PTEN induces a tumor-suppressive metabolic state. Cell **149:**49–62. http://dx.doi.org/10.1016/j.cell.2012.02.030.
31. **Colombo SL, Palacios-Callender M, Frakich N, De Leon J, Schmitt CA, Boorn L, Davis N, Moncada S.** 2010. Anaphase-promoting complex/cyclosome-Cdh1 coordinates glycolysis and glutaminolysis with transition to S phase in human T lymphocytes. Proc. Natl. Acad. Sci. U. S. A. **107:**18868–18873. http://dx.doi.org/10.1073/pnas.1012362107.
32. **Najafov A, Alessi DR.** 2010. Uncoupling the Warburg effect from cancer. Proc. Natl. Acad. Sci. U. S. A. **107:**19135–19136. http://dx.doi.org/10.1073/pnas.1014047107.
33. **Song MS, Salmena L, Pandolfi PP.** 2012. The functions and regulation of the PTEN tumour suppressor. Nat. Rev. Mol. Cell. Biol. **13:**283–296. http://dx.doi.org/10.1038/nrm3330.
34. **Lee JT, Shan J, Zhong J, Li M, Zhou B, Zhou A, Parsons R, Gu W.** 2013. RFP-mediated ubiquitination of PTEN modulates its effect on AKT activation. Cell Res. **23:**552–564. http://dx.doi.org/10.1038/cr.2013.27.
35. **Maddika S, Kavela S, Rani N, Palicharla VR, Pokorny JL, Sarkaria JN, Chen J.** 2011. WWP2 is an E3 ubiquitin ligase for PTEN. Nat. Cell Biol. **13:**728–733. http://dx.doi.org/10.1038/ncb2240.
36. **Wang X, Trotman LC, Koppie T, Alimonti A, Chen Z, Gao Z, Wang J, Erdjument-Bromage H, Tempst P, Cordon-Cardo C, Pandolfi PP, Jiang X.** 2007. NEDD4-1 is a proto-oncogenic ubiquitin ligase for PTEN. Cell **128:**129–139. http://dx.doi.org/10.1016/j.cell.2006.11.039.
37. **Zhang XC, Piccini A, Myers MP, Van Aelst L, Tonks NK.** 2012. Functional analysis of the protein phosphatase activity of PTEN. Biochem. J. **444:**457–464. http://dx.doi.org/10.1042/BJ20120098.
38. **Li H, Wang Y, Liu X.** 2008. Plk1-dependent phosphorylation regulates functions of DNA topoisomerase IIalpha in cell cycle progression. J. Biol. Chem. **283:**6209–6221. http://dx.doi.org/10.1074/jbc.M709007200.
39. **Liu X, Erikson RL.** 2003. Polo-like kinase (Plk)1 depletion induces apoptosis in cancer cells. Proc. Natl. Acad. Sci. U. S. A. **100:**5789–5794. http://dx.doi.org/10.1073/pnas.1031523100.
40. **Lei M, Erikson RL.** 2008. Plk1 depletion in nontransformed diploid cells activates the DNA-damage checkpoint. Oncogene **27:**3935–3943. http://dx.doi.org/10.1038/onc.2008.36.
41. **Song B, Liu XS, Davis K, Liu X.** 2011. Plk1 phosphorylation of Orc2 promotes DNA replication under conditions of stress. Mol. Cell. Biol. **31:**4844–4856. http://dx.doi.org/10.1128/MCB.06110-11.
42. **Wu ZQ, Liu X.** 2008. Role for Plk1 phosphorylation of Hbo1 in regulation

of replication licensing. Proc. Natl. Acad. Sci. U. S. A. **105:**1919–1924. http://dx.doi.org/10.1073/pnas.0712063105.

43. **Yang Y, Bai J, Shen R, Brown SA, Komissarova E, Huang Y, Jiang N, Alberts GF, Costa M, Lu L, Winkles JA, Dai W.** 2008. Polo-like kinase 3 functions as a tumor suppressor and is a negative regulator of hypoxia-inducible factor-1 alpha under hypoxic conditions. Cancer Res. **68:**4077–4085. http://dx.doi.org/10.1158/0008-5472.CAN-07-6182.
44. **Choi B, Pagano M, Dai W.** 2014. Plk1 phosphorylates PTEN and regulates its mitotic activity during the cell cycle. J. Biol. Chem. **289:**14066–14074. http://dx.doi.org/10.1074/jbc.M114.558155.
45. **Li H, Liu XS, Yang X, Wang Y, Turner JR, Liu X.** 2010. Phosphorylation of CLIP-170 by Plk1 and CK2 promotes timely formation of kinetochore-microtubule attachments. EMBO J. **29:**2953–2965. http://dx.doi.org/10.1038/emboj.2010.174.